Ferromagnet - Superconductor Hybrids

I. F. Lyuksyutov and V. L. Pokrovsky
Department of Physics, Texas A&M University

July 6, 2004

Abstract

A new class of phenomena discussed in this review is based on interaction between spatially separated, but closely located ferromagnets and superconductors. They are called Ferromagnet-Superconductor Hybrids (FSH). These systems include coupled smooth and textured Ferromagnetic and Superconducting films, magnetic dots, wires etc. The interaction may be provided by the magnetic flux from magnetic textures and supercurrents. The magnetic flux from magnetic textures or topological defects can pin vortices or create them, changing drastically the properties of the superconductor. On the other hand, the magnetic field from supercurrents (vortices) strongly interacts with the magnetic subsystem leading to formation of coupled magnetic-superconducting topological defects. We discuss possible experimental realization of the FSH. The presence of ferromagnetic layer can change dramatically the properties of the superconducting film due to proximity effect. We discuss experimental and theoretical studies of the proximity effect in the FSH including transition temperature, order parameter oscillations and triplet superconductivity.

Contents

1 Introduction

In this review we discuss a new avenue in solid state physics: studies of physical phenomena which appear when two mutually exclusive states of matter, superconductivity and ferromagnetism, are combined in an unified Ferromagnet-Superconductor Hybrid (FSH) system. In the hybrid systems fabricated from materials with different and even mutually exclusive properties, a strong mutual interaction between subsystems can dramatically change properties of the constituent materials. This approach offers vast opportunities for science and technology. The interplay of superconductivity and ferromagnetism has been thoroughly studied experimentally and theoretically [1, 2] for homogeneous systems. In such systems, both order parameters are homogeneous in space and suppress each other. As a result, one or both the orderings are weak. A natural way to avoid the mutual suppression of the order parameter of the superconducting (S) and ferromagnetic (F) subsystems is to separate them by a thin but impenetrable insulator film. In such systems the S and F subsystems interact via magnetic field induced by the nonuniform magnetization of the F textures penetrating into the superconductor. If this field is strong enough, it can generate vortices in the superconductor. The textures can be either artificial (dots, wires) or topological like Domain Walls (DW). The inverse effect is also important: the S currents generate magnetic field interacting with the magnetization in F subsystem.

First experimental works on FSH were focused on pinning properties of magnetic dot arrays covered by a thin superconducting film [3, 4, 5, 6, 7]. The effect of commensurability on the transport properties was reported in [3, 4, 5, 6]. This effect is not specific for magnets interacting with superconductors and was first observed in textured superconducting films. First experiments with such films were performed in seventies. In these experiments the periodicity of the vortex lattice fixed by external magnetic field competed with the periodicity of an artificial array created by experimenters. Martinoli *et al.* [8, 9, 10] used grooves and Hebard *et al.* [11, 12] used arrays of holes. This approach was further developed by experimentalists in nineties [13]-[19]. Theoretical analysis was also performed in the last century [20, 21, 22]. First observation of the dependence of vortex pinning by magnetic dots array on the magnetic field direction was presented by Morgan and Ketterson [7]. This was first direct indication of new physics in FSH. New insight into the FSH physics has been provided by Magnetic Force Microscope (MFM) and Scanning Hall Probe Microscope (SHPM). By using such imaging technique the group at the University of Leuven has elucidated several pinning mechanisms in FSH [23]-[25].

Different mesoscopic magneto-superconducting systems were proposed and studied theoretically: arrays of magnetic dots on the top of a SC film [26, 27, 28, 29], Ferromagnet-Superconductor Bilayer (FSB) [28, 30, 31, 32, 33, 34], embedded magnetic nanowires combined with bulk superconductor [35, 36] or superconductor film [37, 38], a layer of magnetic dipoles between two bulk superconductors [39], an array of magnetic dipoles mimicking the FM dots on SC film [40], "giant" magnetic dot which generates several vortices in bulk superconductor [41], single magnetic dots on a thin superconducting film [42, 43, 44, 45, 46], thick magnetic film combined with thick [47, 48, 49, 50] or thin superconducting film [51, 52].

The characteristic scale scale of the magnetic field and current variation in all mentioned

systems significantly exceeds the coherence length ξ. It means that they can be considered in London approximation with good precision. In the next section we derive basic equations describing FSH. Starting from London-Maxwell equations, we derive a variational principle (energy) containing only the values inside either S or F components. These equations allowed us to study single magnetic dots coupled with superconducting film (Sec. 3.1) as well as arrays of such dots (Section 3.2). The simplest possible FSH system - sandwich formed by Ferromagnetic and Superconducting layers, divided by ultrathin insulating film (FSB),- can demonstrate unusual behavior: spontaneous formation of coupled system of vortices and magnetic domains. These phenomena are discussed in Section 3.3. We also discuss the influence of the thick magnetic film on the bulk superconductor.

An alternative approach to heterogeneous SC/FM systems is just to employ the proximity effects instead of avoiding them. The exchange field existing in the ferromagnet splits the Fermi spheres for up and down spins. Thus, the Cooper pair acquires a non-zero total momentum and its wave function oscillates in space. This effect first predicted by Larkin and Ovchinnikov [53] and by Ferrel and Fulde [54] will be cited further as LOFF effect. One of its manifestation is the change of sign of the Cooper pair tunneling amplitude in space. At some conditions the Josephson current through a superconductor-ferromagnet-superconductor (S/F/S) junction has sign opposite to $\sin\varphi$, where φ is the phase difference between right and left superconducting layers. This type of junctions was first proposed theoretically long time ago by Bulaevsky *et al.* [55], [56] and was called π-junction in contrast to standard or 0-junction. It was first reliably realized in the experiment by Ryazanov and coworkers in 2001 [57, 58] and a little later by Kontos *et al.* [59]. The experimental findings of these groups have generated an extended literature. A large exhausting review on this topic was published in the beginning of 2002 [60]. A more special survey was published at the same time by Garifullin [61]. We are not going to repeat what was already done in this reviews and will focus presumably on works which appeared after its publication. Only basic notions and ideas necessary for understanding will be extracted from previous works.

Most of the proximity phenomena predicted theoretically and found experimentally are based on the oscillatory behavior of the Cooper pair wave function. These are the oscillations of the transition temperature (first predicted in [62, 63]), and the critical current vs. the thickness of ferromagnetic layer which are seen as oscillatory transitions from 0- to π-junctions [56]. Other proximity effects besides the usual suppression of the order parameters include the preferential antiparallel orientation of the F-layers in a F/S/F trilayer, the so-called spin-valve effect [64, 65, 66].

More recently a new idea was proposed by Kadigrobov *et al.* [67] and by Bergeret, Efetov and Volkov [68]: they have predicted that the magnetization varying its direction in space transforms singlet Cooper pairs into triplet ones. The triplet pairing is not suppressed by the exchange field and can propagate in the ferromagnet on large distances thus providing the long-range proximity between superconductors in S/F/S junctions.

The proximity effects may have technological applications as elements of high-speed magnetic electronics based on the spin valve action [66] and also as elements of quantum computers [69]. Purely magnetic interaction between ferromagnetic and superconducting sub-

systems can also be used to design magnetic field controlled superconducting devices. A magnetic field controlled Josephson interferometer in a thin magnetic F/S bilayer has been demonstrated by Eom and Johnson [70].

In the next Section we derive basic equations. Third Section is focused on phenomena in FSH which are based on only magnetic interaction between ferromagnetic and superconducting subsystem. Recent results on proximity based phenomena in bi- and tri-layer FSH are presented in the last Section.

2 Basic Equations

In the proposed and experimentally realized FSH a magnetic texture interacts with the supercurrent. First we assume that ferromagnetic and superconducting subsystems are separated by thin insulating layer which prevents proximity effect, focusing on magnetic interaction only. Inhomogeneous magnetization generates magnetic field outside the ferromagnets. This magnetic field generates screening currents in superconductors which, in turn, change the magnetic field. The problem must be solved self-consistently. The calculation of the vortex and magnetization arrangement for interacting, spatially separated superconductors and ferromagnets is based on the static London-Maxwell equations and corresponding energy. This description includes possible superconducting vortices. Londons approximation works satisfactory since the sizes of all structures in the problem exceed significantly the coherence length ξ. We remind that in the Londons approximation the modulus of the order parameter is constant and the phase varies in space. Starting from the London-Maxwell equation in all the space, we eliminate the magnetic field outside their sources and obtain equations for the currents, magnetization and fields inside them. This is done in the subsection 2.1. In the subsection 2.2 we apply this method to the case of very thin coupled ferromagnetic and superconducting films. When proximity effects dominate, the Londons approximation is invalid. The basic equations for this case will be described in subsection 2.3.

2.1 Three-Dimensional Systems.

The total energy of a stationary F-S system reads:

$$H = \int [\frac{\mathbf{B}^2}{8\pi} + \frac{m_s n_s \mathbf{v}_s^2}{2} - \mathbf{B}\cdot\mathbf{M}]dV \tag{1}$$

where $\mathbf{B}$ is the magnetic induction, $\mathbf{M}$ is the magnetization, n_s is the density of S-electrons, m_s is their effective mass and $\mathbf{v}_s$ is their velocity. We assume that the SC density n_s and the magnetization $\mathbf{M}$ are separated in space. We assume also that the magnetic field $\mathbf{B}$ and its vector-potential $\mathbf{A}$ asymptotically turn to zero at infinity. Employing static Maxwell equation $\nabla \times \mathbf{B} = \frac{4\pi}{c}\mathbf{j}$, and $\mathbf{B} = \nabla \times \mathbf{A}$, the magnetic field energy can be transformed as follows:

$$\int \frac{\mathbf{B}^2}{8\pi} dV = \int \frac{\mathbf{j}\cdot\mathbf{A}}{2c} dV \tag{2}$$

Though the vector-potential enters explicitly in the last equation, it is gauge invariant due to the current conservation div$\mathbf{j} = 0$. When integrating by part, we neglected the surface term. This is correct if the field, vector-potential and the current decrease sufficiently fast at infinity. This condition is satisfied for simple examples considered in this article. The current $\mathbf{j}$ can be represented as a sum: $\mathbf{j} = \mathbf{j}_s + \mathbf{j}_m$ of the SC and magnetic currents, respectively:

$$\mathbf{j}_s = \frac{n_s \hbar e}{2m_s}(\nabla\varphi - \frac{2\pi}{\Phi_0}\mathbf{A}) \tag{3}$$

$$\mathbf{j}_m = c\nabla \times \mathbf{M}. \tag{4}$$

We consider contributions from magnetic and S-currents into the integral (2) separately. We start with the integral:

$$\frac{1}{2c}\int \mathbf{j}_m \mathbf{A} dV = \frac{1}{2}\int (\nabla \times \mathbf{M}) \cdot \mathbf{A} dV \tag{5}$$

Integrating by part and neglecting the surface term again, we arrive at a following result:

$$\frac{1}{2c}\int \mathbf{j}_m \mathbf{A} dV = \frac{1}{2}\int \mathbf{M} \cdot \mathbf{B} dV \tag{6}$$

We have omitted the integral over a remote surface $\oint(\mathbf{n} \times \mathbf{M}) \cdot \mathbf{A} dS$. Such an omission is valid if the magnetization is confined to a limited volume. But for infinite magnetic systems it may be wrong even in simplest problems. We will discuss such a situation in the next section.

Next we consider the contribution of the superconducting current $\mathbf{j}_s$ to the integral (2). In the gauge-invariant equation 3 φ is the phase of the S-carriers (Cooper pairs) wave-function and $\Phi_0 = hc/2e$ is the flux quantum. Note that the phase gradient $\nabla\varphi$ can be included into $\mathbf{A}$ as a gauge transformation with exception of vortex lines, where φ is singular. We employ equation (3) to express the vector-potential $\mathbf{A}$ in terms of the supercurrent and the phase gradient:

$$\mathbf{A} = \frac{\Phi_0}{2\pi}\nabla\varphi - \frac{m_s c}{n_s e^2}\mathbf{j}_s \tag{7}$$

Plugging equation (7) into equation (2), we find:

$$\frac{1}{2c}\int \mathbf{j}_s \mathbf{A} dV = \frac{\hbar}{4e}\int \nabla\varphi \cdot \mathbf{j}_s dV - \frac{m_s}{2n_s e^2}\int j_s^2 dV \tag{8}$$

Since $\mathbf{j}_s = e n_s \mathbf{v}_s$, the last term in this equation is equal to the kinetic energy taken with the sign minus. It exactly compensates the kinetic energy in the initial expression for the energy (1). Collecting all remaining terms, we obtain a following expression for the total energy:

$$H = \int [\frac{n_s \hbar^2}{8m_s}(\nabla\varphi)^2 - \frac{n_s \hbar e}{4m_s c}\nabla\varphi \cdot \mathbf{A} - \frac{\mathbf{B} \cdot \mathbf{M}}{2}] dV \tag{9}$$

We remind again about a possible surface term for infinite magnetic systems. Note that integration in the expression for energy (9) proceeds over the volumes occupied either by

superconductors or by magnets. Equation (9) allows to separate the energy of vortices from the energy of magnetization induced currents and fields and their interaction energy. Indeed, as we noted earlier, the phase gradient can be ascribed to the contribution of vortex lines only. It is representable as a sum of independent integrals over different vortex lines. The vector-potential and the magnetic field can be represented as a sum of magnetization induced and vortex induced parts: $\mathbf{A} = \mathbf{A}_m + \mathbf{A}_v$, $\mathbf{B} = \mathbf{B}_m + \mathbf{B}_v$, where $\mathbf{A}_k$, $\mathbf{B}_k$ (the index k is either m or v) are determined as solutions of the Londons-Maxwell equations:

$$\nabla \times (\nabla \times \mathbf{A}_k) = \frac{4\pi}{c}\mathbf{j}_k, \tag{10}$$

The effect of the screening of magnetic field generated by magnetization by superconductor is included into the vector fields $\mathbf{A}_m$ and $\mathbf{B}_m$. Applying such a separation, we present the total energy (9) as a sum of terms containing only vortex contributions, only magnetic contributions and the interaction terms. The purely magnetic part can be represented as a nonlocal quadratic form of the magnetization. The purely superconducting part is representable as a non-local double integral over the vortex lines. Finally, the interaction term is representable as a double integral which proceeds over the vortex lines and the volume occupied by the magnetization and is bi-linear in magnetization and vorticity. To avoid cumbersome formulas, we will not write these expressions explicitly.

2.2 Two-Dimensional Systems.

Below we perform a more explicit analysis for the case of two parallel films, one F, another S, both very thin and very close to each other. Neglecting their thickness, we assume that both films are located approximately at $z = 0$. In some cases we need a more accurate treatment. Then we introduce a small distance d between films which in the end will be put zero. Though the thickness of each film is assumed to be small, the 2-dimensional densities of S-carriers $n_s^{(2)} = n_s d_s$ and magnetization $\mathbf{m} = \mathbf{M} d_m$ remain finite. Here we introduced the thickness of the S film d_s and the F film d_m. The 3d super-carrier density $n_s(\mathbf{R})$ can be represented as $n_s(\mathbf{R}) = \delta(z) n_s^{(2)}(\mathbf{r})$ and the 3d magnetization $\mathbf{M}(\mathbf{R})$ can be represented as $\mathbf{M}(\mathbf{R}) = \delta(z-d)\mathbf{m}(\mathbf{r})$, where $\mathbf{r}$ is the two-dimensional radius-vector and z-direction is perpendicular to the films. In what follows $n_s^{(2)}$ is assumed to be a constant and the index (2) is omitted. The energy (9) can be rewritten for this special case:

$$H = \int [\frac{n_s \hbar^2}{8 m_s}(\nabla\varphi)^2 - \frac{n_s \hbar e}{4 m_s c}\nabla\varphi \cdot \mathbf{a} - \frac{\mathbf{b}\cdot\mathbf{m}}{2}] d^2\mathbf{r} \tag{11}$$

where $\mathbf{a} = \mathbf{A}(\mathbf{r}, z=0)$ and $\mathbf{b} = \mathbf{B}(\mathbf{r}, z=0)$. The vector-potential satisfies Maxwell-Londons equation:

$$\begin{aligned} \nabla \times (\nabla \times \mathbf{A}) &= -\frac{1}{\lambda}\mathbf{A}\delta(z) + \frac{2\pi\hbar n_s e}{m_s c}\nabla\varphi\delta(z) \\ &+ 4\pi\nabla \times (\mathbf{m}\delta(z)) \end{aligned} \tag{12}$$

Here $\lambda = \lambda_L^2/d_S$ is the effective screening length for the S film, λ_L is the London penetration depth and d_s is the S-film thickness[71].

According to our general arguments, the term proportional to $\nabla\varphi$ in equation (13) describes vortices. A plane vortex characterized by its vorticity q and by the position of its center on the plane $\mathbf{r}_0$ contributes a singular term to $\nabla\varphi$:

$$\nabla\varphi_0(\mathbf{r},\mathbf{r}_0) = q\frac{\hat{z}\times(\mathbf{r}-\mathbf{r}_0)}{|\mathbf{r}-\mathbf{r}_0|^2} \tag{13}$$

and generates a standard vortex vector-potential:

$$\begin{aligned}\mathbf{A}_{v0}(\mathbf{r}-\mathbf{r}_0,z) &= \frac{q\Phi_0}{2\pi}\frac{\hat{z}\times(\mathbf{r}-\mathbf{r}_0)}{|\mathbf{r}-\mathbf{r}_0|} \\ &\times \int_0^\infty \frac{J_1(k|\mathbf{r}-\mathbf{r}_0|)e^{-k|z|}}{1+2k\lambda}dk\end{aligned} \tag{14}$$

Different vortices contribute independently into the vector-potential and magnetic field. A peculiarity of this problem is that the usually applied gauge div$\mathbf{A} = 0$ becomes singular in the limit $d_s, d_m \to 0$. Therefore, it is reasonable to apply another gauge $A_z = 0$. The calculations are much simpler in Fourier-representation. Following the general procedure, we present the Fourier-transform of the vector-potential $\mathbf{A}_\mathbf{k}$ as a sum $\mathbf{A}_\mathbf{k} = \mathbf{A}_{m\mathbf{k}} + \mathbf{A}_{v\mathbf{k}}$. Equation for the magnetic part of the vector-potential reads:

$$\mathbf{k}(\mathbf{q}\mathbf{A}_{m\mathbf{k}}) - k^2\mathbf{A}_{m\mathbf{k}} = \frac{\mathbf{a}_{m\mathbf{q}}}{\lambda} - 4\pi i\mathbf{k}\times\mathbf{m}_\mathbf{q}e^{ik_zd} \tag{15}$$

where $\mathbf{q}$ is projection of the wave vector $\mathbf{k}$ onto the plane of the films: $\mathbf{k} = k_z\hat{z} + \mathbf{q}$. An arbitrary vector field $\mathbf{V}_\mathbf{k}$ in the wave-vector space can be represented by its local coordinates:

$$\mathbf{V}_\mathbf{k} = V_\mathbf{k}^z\hat{z} + V_\mathbf{k}^\parallel\hat{q} + V_\mathbf{k}^\perp(\hat{z}\times\hat{q}) \tag{16}$$

In terms of these coordinates the solution of equation (15) reads:

$$A_{m\mathbf{k}}^\parallel = -\frac{4\pi i m_\mathbf{q}^\perp}{k_z}e^{ik_zd} \tag{17}$$

$$A_{m\mathbf{k}}^\perp = -\frac{1}{\lambda k^2}a_\mathbf{q}^\perp + \frac{4\pi i\left(k_zm_\mathbf{q}^\parallel - qm_{\mathbf{q}z}\right)}{k^2}e^{ik_zd} \tag{18}$$

Integration of the latter equation over k_z allows to find the perpendicular component of $\mathbf{a}_\mathbf{q}{}^{(m)}$:

$$a_{m\mathbf{q}}^\perp = -\frac{4\pi\lambda q(m_\mathbf{q}^\parallel + im_{\mathbf{q}z})}{1+2\lambda q}e^{-qd}, \tag{19}$$

whereas it follows from equation (15) that $a_{m\mathbf{q}}^\parallel = 0$. Note that the parallel component of the vector-potential $A_{m\mathbf{k}}^\parallel$ does not know anything about the S film. It corresponds to the

magnetic field equal to zero outside the plane of F film. Therefore, it is inessential for our problem.

The vortex part of the vector-potential also does not contain z-component since the supercurrents flow in the plane. The vortex solution in a thin film was first found by Pearl [72]. An explicit expression for the vortex-induced potential is:

$$\mathbf{A}_{v\mathbf{k}} = \frac{2i\Phi_0(\hat{z}\times\hat{q})F(\mathbf{q})}{\mathbf{k}^2(1+2\lambda q)}, \tag{20}$$

where $F(\mathbf{q}) = \sum_j e^{i\mathbf{q}\mathbf{r}_j}$ is the vortex form-factor; the index j labels the vortices and $\mathbf{r}_j$ are coordinates of the vortex centers. The Fourier-transformation for the vortex-induced vector-potential at the surface of the SC film $\mathbf{a}_{v\mathbf{q}}$ reads:

$$\mathbf{a}_{v\mathbf{q}} = \frac{i\Phi_0(\hat{z}\times\hat{q})F(\mathbf{q})}{q(1+2\lambda q)} \tag{21}$$

The z-component of magnetic field induced by the Pearl vortex in real space is:

$$B_{vz} = \frac{\Phi_0}{2\pi}\int_0^\infty \frac{J_0(qr)e^{-q|z|}}{1+2\lambda q}qdq \tag{22}$$

Its asymptotic at $z=0$ and $r \gg \lambda$ is $B_{vz} \approx \Phi_0\lambda/(\pi r^3)$; at $r \ll \lambda$ it is $B_{vz} \approx \Phi_0/(\pi\lambda r)$. Each Pearl vortex carries the flux quantum $\Phi_0 = \pi\hbar c/e$.
The energy (11), can be expressed in terms of Fourier-transforms:

$$H = H_v + H_m + H_{vm}, \tag{23}$$

where purely vortex energy H_v is the same as it would be in the absence of the FM film:

$$H_v = \frac{n_s\hbar^2}{8m_s}\int \nabla\varphi_{-\mathbf{q}}(\nabla\varphi_{\mathbf{q}} - \frac{2\pi}{\Phi_0}\mathbf{a}_{v\mathbf{q}})\frac{d^2q}{(2\pi)^2}; \tag{24}$$

The purely magnetic energy H_m is:

$$H_m = -\frac{1}{2}\int \mathbf{m}_{\mathbf{q}}\mathbf{b}_{m\mathbf{q}} \tag{25}$$

It contains the screened magnetic field and therefore differs from its value in the absence of the SC film . Finally the interaction energy reads:

$$\begin{aligned} H_{mv} &= -\frac{n_s\hbar e}{4m_s c}\int(\nabla\varphi)_{-\mathbf{q}}\mathbf{a}_{m\mathbf{q}}\frac{d^2q}{(2\pi)^2} \\ &- \frac{1}{2}\int \mathbf{m}_{-\mathbf{q}}\mathbf{b}_{v\mathbf{q}}\frac{d^2q}{(2\pi)^2} \end{aligned} \tag{26}$$

Note that the information on the vortex arrangement is contained in the form-factor $F(\mathbf{q})$ only.

To illustrate how important can be the surface term, let consider a homogeneous perpendicularly magnetized magnetic film and one vortex in superconducting film. The authors [30] have shown that the energy of this system is $\varepsilon_v = \varepsilon_v^0 - m\Phi_0$, where ε_v^0 is the energy of the vortex in the absence of magnetic film, m is the magnetization per unit area and $\Phi_0 = hc/2e$ is the magnetic flux quantum. Let consider how this result appears from the microscopic calculations. The vortex energy (24) is just equal to ε_v^0. Purely magnetic term (25) does not change in the presence of vortex and is inessential. The first term in the interaction energy (26) is equal to zero since the infinite magnetic film does not generate magnetic field outside. The second term of this energy is equal to $-m\Phi_0/2$. The second half of the interaction energy comes from the surface term. Indeed, it is equal to

$$\begin{aligned}(1/2)\lim_{r\to\infty}\int_0^{2\pi} m(\hat{r}\times\hat{z})\cdot\mathbf{A}rd\varphi &= -(1/2)\oint\mathbf{A}\cdot d\mathbf{r}\\ &= -m\Phi_0/2\end{aligned}$$

2.3 Eilenberger and Usadel Equations

The essence of proximity phenomena is the change of the order parameter (Cooper pair wave function). Therefore, the London approximation is not valid in this case and equations for the order parameter must be solved. They are either Bogolyubov-DeGennes equations [73, 74] for the coefficients u and v or more conveniently the Gor'kov equations [75] for Green functions. Unfortunately the solution of these equations is not an easy problem in the spatially inhomogeneous case combined with the scattering by impurities and/or irregular boundaries. This is a typical situation for the experiments with F/S proximity effects, since the layers are thin, the diffusion delivers atoms of one layer into another and the control of the structure and morphology is not so strict as for 3d single crystals. Sometimes experimenters deliberately use amorphous alloys as magnetic layers [76]. Fortunately, if the scale of variation for the order parameter is much larger than atomic, the semiclassical approximation can be applied. Equations for the superconducting order parameter in semiclassical approximation were derived long time ago by Eilenberger [77] and by Larkin and Ovchinnikov [78]. They were further simplified in the case of strong elastic scattering (diffusion approximation) by Usadel [79]. For the reader convenience and for the unification of notations we demonstrate them here referring the reader for derivation to original works or to the textbooks [80, 81].

The Eilenberger equations are written for the electronic Green functions integrated in the momentum space over the momentum component perpendicular to the Fermi surface. Thus, they depend on a point of the Fermi-surface characterized by two momentum components, on the coordinates in real space and time. It is more convenient in thermodynamics to use their Fourier-components over the imaginary time, the so-called Matsubara representation [82]. The frequencies in this representation accept discrete real values $\omega_n = (2n+1)\pi T$, where T is the temperature. The case of singlet pairing is described by two Eilenberger anomalous Green functions $F(\omega, \mathbf{k}, \mathbf{r})$ and $F^\dagger(\omega, \mathbf{k}, \mathbf{r})$ (integrated along the normal to the Fermi-surface Gor'kov anomalous functions), where ω stays for ω_n, $\mathbf{k}$ is the wave vector at

the Fermi sphere and $\mathbf{r}$ is the vector indicating at a point in real space (the coordinate of the Cooper pair center-of-mass). The function F generally is complex in contrast to the integrated normal Green function $G(\omega, \mathbf{k}, \mathbf{r})$, which is real. Eilenberger has proved that the functions G and F are not independent: they obey the normalization condition:

$$[G(\omega, \mathbf{k}, \mathbf{r})]^2 + |F(\omega, \mathbf{k}, \mathbf{r})|^2 = 1 \tag{27}$$

Besides, the Eilenberger Green functions obey the following symmetry relations:

$$F(\omega, \mathbf{k}, \mathbf{r}) = F^*(-\omega, \mathbf{k}, \mathbf{r}) = F^*(\omega, -\mathbf{k}, \mathbf{r}) \tag{28}$$

$$G(-\omega, \mathbf{k}, \mathbf{r}) = -\mathbf{G}^*(\omega, \mathbf{k}, \mathbf{r}) = -\mathbf{G}(\omega, -\mathbf{k}, \mathbf{r}) \tag{29}$$

Eilenberger equations read:

$$\left[2\omega + \mathbf{v}\left(\frac{\partial}{\partial \mathbf{r}} - i\frac{2e}{c}\mathbf{A}(\mathbf{r})\right)\right] F(\omega, \mathbf{k}, \mathbf{r}) = 2\Delta G(\omega, \mathbf{k}, \mathbf{r}) + \int d^2q\rho(\mathbf{q})W(\mathbf{k}, \mathbf{q})[G(\mathbf{k})F(\mathbf{q}) - F(\mathbf{k})G(\mathbf{q})] \tag{30}$$

where $\Delta(\mathbf{r})$ is the space (and time)- dependent order parameter (local energy gap); $\mathbf{v}$ is the velocity on the Fermi surface; $W(\mathbf{k}, \mathbf{q})$ is the probability of transition per unit time from the state with the momentum $\mathbf{q}$ to the state with the momentum $\mathbf{k}$ and $\rho(\mathbf{q})$ is the angular dependence of the density of states normalized by $\int d^2q\rho(\mathbf{q}) = N(0)$. Here $N(0)$ is the total density of states (DOS) in the normal state at the Fermi level. The Eilenberger equations have the structure of Boltzmann kinetic equation, but they also incorporate quantum coherence effects. They must be complemented by the self-consistency equation expressing local value of $\Delta(\mathbf{r})$ in terms of the anomalous Green function F:

$$\Delta(\mathbf{r})\ln(\frac{T}{T_c}) + 2\pi T\sum_{n=0}^{\infty}\left[\frac{\Delta(\mathbf{r})}{\omega_n} - \int d^2k\rho(\mathbf{k})F(\omega_n, \mathbf{k}, \mathbf{r})\right] = 0 \tag{31}$$

In a frequently considered by theorists case of the isotropic scattering the collision integral in equation (30) is remarkably simplified:

$$\int d^2q\rho(\mathbf{q})W(\mathbf{k}, \mathbf{q})[G(\mathbf{k})F(\mathbf{q}) - F(\mathbf{k})G(\mathbf{q})] = \frac{1}{\tau}\left[G(\mathbf{k})\langle F\rangle - F(\mathbf{k})\langle G\rangle\right], \tag{32}$$

where the relaxation time τ is equal to inverse value of angular independent transition probability W and $\langle ...\rangle$ means the angular average over the Fermi sphere.
The Eilenberger equation is simpler than complete Gor'kov equations since it contains only one function depending on by one less number of arguments. It could be expected that in the limit of very short relaxation time $T_{c0}\tau \ll 1$ (T_{c0} is transition temperature in the clean superconductor) the Eilenberger kinetic-like equation will become similar to diffusion equation. Such a diffusion-like equation was indeed derived by Usadel [79]. In the case of strong elastic scattering and the isotropic Fermi surface (sphere) the Green function does

not depend on the direction on the Fermi sphere and depends only on frequency and the spatial coordinate $\mathbf{r}$. The Usadel equation reads (we omit both arguments):

$$2\omega F - D\hat{\partial}\left(G\hat{\partial}F - F\hat{\partial}G\right) = 2\Delta G \tag{33}$$

In this equation $D = v_F^2\tau/3$ is the diffusion coefficient for electrons in the normal state and $\hat{\partial}$ stays for the gauge-invariant gradient: $\hat{\partial} = \nabla - 2ie\mathbf{A}/\hbar c$. The Usadel equations must be complemented by the same self-consistency equation (31). It is also useful to keep in mind expression for the current density in terms of the function F:

$$\mathbf{j} = ie2\pi TN(0)D\sum_{\omega_n>0}(F^*\hat{\partial}F - F\hat{\partial}F^*). \tag{34}$$

One can consider the set of Green functions G, F, $F^\dagger$ as elements of the 2x2 matrix Green function $\hat{g}$ where the matrix indices can be identified with the particle and hole or Nambu channels. This formal trick becomes rather essential when the singlet and triplet pairing coexist and it is necessary to take in account the Nambu indices and spin indices simultaneously. Eilenberger in his original article [77] has indicated a way to implement the spin degrees of freedom in his scheme. Below we demonstrate a convenient modification of this representation proposed by Bergeret *et al.* [83]. Let us introduce a matrix $\check{g}(\mathbf{r},t;\mathbf{r}',t')$ with matrix elements $g_{s,s'}^{n,n'}$, where n,n' are the Nambu indices and s,s' are the spin indices, defined as follows:

$$g_{s,s'}^{n,n'}(\mathbf{r},t;\mathbf{r}',t') = \frac{1}{\hbar}\sum_{n''}(\hat{\tau}_3)_{n,n''}\int d\xi\langle\psi_{n''s}(\mathbf{r},t)\psi_{n's'}^\dagger(\mathbf{r}',t')\rangle \tag{35}$$

The matrix $\hat{\tau}_3$ in the definition (35) is the Pauli matrix in the Nambu space. To clarify the Nambu indices we write explicitly what do they mean in terms of the electronic ψ-operators: $\psi_{1s}\equiv\psi_s;\psi_{2s}\equiv\psi_{\bar{s}}^\dagger$ and $\bar{s}$ means $-s$. The most general matrix $\check{g}$ can be expanded in the Nambu space into a linear combination of 4 independent matrices $\hat{\tau}_k; k = 0,1,2,3$, where $\hat{\tau}_0$ is the unit matrix and three others are the standard Pauli matrices. Following [83], we accept following notations for the components of this expansion, which are matrices in the spin space[1]:

$$\check{g} = \hat{g}_0\hat{\tau}_0 + \hat{g}_3\hat{\tau}_3 + \check{f}; \check{f} = \hat{f}_1 i\hat{\tau}_1 + \hat{f}_2 i\hat{\tau}_2 \tag{36}$$

The matrix $\check{f}$ describes Cooper pairing since it contains only anti-diagonal matrices in the Nambu space. In turn the spin matrices $\hat{f}_1$ and $\hat{f}_2$ can be expanded in the basis of spin Pauli matrices $\sigma_j; j = \hat{0},1,2,3$. Without loss of generality we can accept the following agreement about the scalar components of the spin-space expansion:

$$\hat{f}_1 = f_1\hat{\sigma}_1 + f_2\hat{\sigma}_2; \hat{f}_2 = f_0\hat{\sigma}_0 + f_3\hat{\sigma}_3. \tag{37}$$

It is easy to check that the amplitudes $f_i; i = 0...3$ are associated with the following combinations of the wave-function operators:

$$f_0 \;\rightarrow\; \langle\psi_\uparrow\psi_\downarrow + \psi_\downarrow\psi_\uparrow\rangle$$

[1]Each time when Nambu and spin matrices stay together we mean the direct product.

$$
\begin{aligned}
f_1 &\rightarrow \langle \psi_\uparrow \psi_\uparrow - \psi_\downarrow^\dagger \psi_\downarrow^\dagger \rangle \\
f_2 &\rightarrow \langle \psi_\uparrow \psi_\uparrow + \psi_\downarrow^\dagger \psi_\downarrow^\dagger \rangle \\
f_3 &\rightarrow \langle \psi_\uparrow \psi_\downarrow - \psi_\downarrow \psi_\uparrow \rangle
\end{aligned}
$$

Thus, the amplitude f_3 corresponds to the singlet pairing, whereas three others are responsible for the triplet pairing. In particular, in the absence of triplet pairing only the component f_3 survives and the matrix $\check{f}$ is equal to

$$
\begin{pmatrix} 0 & F \\ F^\dagger & 0 \end{pmatrix}
$$

Let us consider what modification must be introduced into the Eilenberger and Usadel equations to take in account the exchange interaction of Cooper pairs with the magnetization in the ferromagnet. Neglecting the reciprocal effect of the Cooper pairs onto the electrons of d- or f-shell responsible for magnetization, we introduce the effective exchange field $h(\mathbf{r})$ acting inside the ferromagnet. It produces pseudo-Zeeman splitting of the spin energy[2]. In the case of the singlet pairing the Matsubara frequency ω must be substituted by $\omega + ih(\mathbf{r})$. When the direction of magnetization changes in space generating triplet pairing, the Usadel equation is formulated in terms of the matrix $\check{g}$ [83]:

$$
\frac{D}{2}\partial(\check{g}\partial\check{g}) - |\omega|[\hat{\tau}_3\hat{\sigma}_3, \check{g}] + \mathrm{sign}\omega[\check{h}, \check{g}] = -i[\check{\Delta}, \check{g}], \tag{38}
$$

where the operators of the magnetic field $\check{h}$ and the energy gap $\check{\Delta}$ are defined as follows:

$$
\check{h} = \tau_3 \sigma \cdot \mathbf{h} \tag{39}
$$

$$
\check{\Delta} = \Delta i \tau_2 \sigma_2 \tag{40}
$$

To find a specific solution of the Eilenberger and Usadel equations proper boundary conditions should be formulated. For the Eilenberger equations the boundary conditions at an interface of two metals were derived by Zaitsev [84]. They are most naturally formulated in terms of the antisymmetric ($\check{g}^a$) and symmetric ($\check{g}^s$) parts of the matrix $\check{g}$ with respect to reflection of momentum $p_z \rightarrow -p_z$ assuming that z is normal to the interface. One of them states that the antisymmetric part is continuous at the interface ($z = 0$):

$$
\check{g}^a(z = -0) = \check{g}^a(z = +0) \tag{41}
$$

The second equation connects the discontinuity of the symmetric part at the interface $\check{g}^s_- = \check{g}^s(z = +0) - \check{g}^s(z = -0)$ with the reflection coefficient R and transmission coefficient D of the interface and antisymmetric part $\check{g}^a$ at the boundary:

$$
D\check{g}^s_-(\check{g}^s_+ - \check{g}^a\check{g}^s_-) = R\check{g}^a[1 - (\check{g}^a)^2], \tag{42}
$$

[2]In reality the exchange energy has quite different origin than the Zeeman interaction, but at a fixed magnetization there is a formal similarity in the Hamiltonians.

where $\check{g}^s_+ = \check{g}^c(z=+0) + \check{g}^c(z=-0)$. If the boundary is transparent (R=0, D=1), the symmetric part of the Green tensor $\check{g}$ is also continuous.
The boundary conditions for the Usadel equations, i.e. under the assumption that the mean free path of electron l is much shorter than the coherence length ξ, were derived by Kupriyanov and Lukichev[85]. The first of them ensures the continuity of the current flowing through the interface:

$$\sigma_< \check{g}_< \frac{d\check{g}_<}{dz} = \sigma_> \check{g}_> \frac{d\check{g}_>}{dz}, \tag{43}$$

where the subscripts $<$ and $>$ relate to the left and right sides of the interface; $\sigma_{<,>}$ denote the conductivity of the proper metal. The second boundary condition connects the current with the discontinuity of the order parameter through the boundary and its transmission and reflection coefficients $D(\theta)$ and $R(\theta)$:

$$l_> \check{g}_> \frac{d\check{g}_>}{dz} = \frac{3}{4} \langle \frac{cos\theta D(\theta)}{R(\theta)} \rangle [\check{g}_<, \check{g}_>], \tag{44}$$

where θ is the incidence angle of the electron at the interface and $D(\theta)$, $R(\theta)$ are corresponding transmission and reflection coefficients. This boundary condition can be rewritten in terms of measurable characteristics:

$$\sigma_> \check{g}_> \frac{d\check{g}_>}{dz} = \frac{1}{R_b} \rangle [\check{g}_<, \check{g}_>], \tag{45}$$

where R_b is the resistance of the interface. In the case of high transparency ($R \ll 1$) the boundary conditions (43,44) can be simplified as follows [86]:

$$\check{f}_< = \check{f}_>; \frac{d\check{f}_<}{dz} = \gamma \frac{d\check{f}_>}{dz}, \tag{46}$$

where γ is the ratio of normal state resistivities.

3 Hybrids Without Proximity Effect

3.1 Magnetic Dots

In this subsection we consider the ground state of a SC film with a circular very thin FM dot grown upon it. The magnetization will be considered to be fixed, homogeneous inside the dot and directed either perpendicular or parallel to the SC film (see figure 1). This problem is basic one for a class of more complicated problems incorporating arrays of magnetic dots.

We will analyze what are conditions for appearance of vortices in the ground state, where do they appear and what are magnetic fields and currents in these states. The S film is assumed to be very thin, plane and infinite in the lateral directions. Since the magnetization is confined inside the finite dot no difficulties with the surface integrals over infinitely remote surfaces or contours arise.

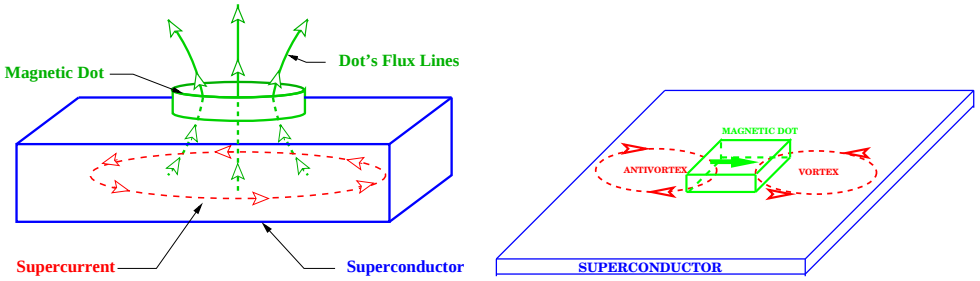

Figure 1: Magnetic dots with out-of-plane and in-plane magnetization and vortices.

3.1.1 Magnetic Dot: Perpendicular magnetization

For an infinitely thin circular magnetic dot of the radius R with 2d magnetization $\mathbf{m}(\mathbf{r}) = m\hat{z}\Theta(R-r)\delta(z-d)$ on the top of the SC film the magnetic field can be calculated using equations (18,19). The Fourier-component of magnetization necessary for this calculation is:

$$\mathbf{m_k} = \hat{z}\frac{2\pi mR}{q}J_1(qR)e^{ik_z d}, \tag{47}$$

where $J_1(x)$ is the Bessel function. The Fourier-transforms of the vector-potential reads:

$$\begin{aligned} A^{\perp}_{m\mathbf{k}} &= -\frac{i8\pi^2 mRJ_1(qR)}{k^2} \\ &\times \quad (e^{-qd}\frac{2q\lambda}{1+2q\lambda} + (e^{ik_z d} - e^{-qd})) \end{aligned} \tag{48}$$

Though the difference in the round brackets in equation (48) looks to be always small (we remind that d must be put zero in the final answer), we can not neglect it since it occurs to give a finite, not small contribution to the parallel component of the magnetic field between the two films. From equation (48) we immediately find the Fourier-transforms of the magnetic field components:

$$B^z_{m\mathbf{q}} = iqA^{\perp}_{m\mathbf{q}}; \;\; B^{\perp}_{m\mathbf{q}} = -ik_z A^{\perp}_{m\mathbf{q}} \tag{49}$$

For the readers convenience we also present the Fourier-transform of the vector-potential at the superconductor surface:

$$a^{\perp}_{m\mathbf{q}} = -\frac{i8\pi^2\lambda mR}{1+2q\lambda}J_1(qR) \tag{50}$$

In the last equation we have put e^{-qd} equal to 1.

Performing inverse Fourier-transformation, we find the magnetic field in real space:

$$B^z_m(r,z) = 4\pi\lambda mR\int_0^{\infty}\frac{J_1(qR)J_0(qr)e^{-q|z|}}{1+2q\lambda}q^2dq \tag{51}$$

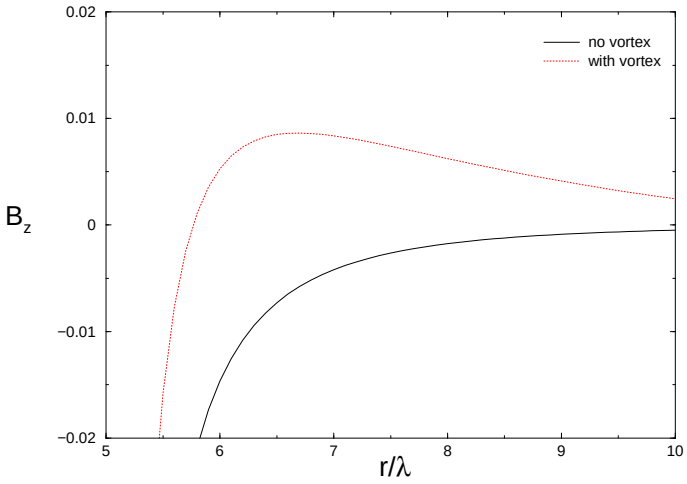

Figure 2: Magnetic field of dot with and without vortex for $R/\lambda = 5$ and $\Phi_0/8\pi^2 mR = 4$

$$B_m^r \quad (\mathbf{r}, z) = 2\pi mR \int_0^\infty J_1(qR) J_1(qr) e^{-q|z|}$$
$$\times \quad [\frac{2q\lambda}{1+2q\lambda}\Theta(z) + \Theta(z-d) - \Theta(z)] q dq, \tag{52}$$

where $\Theta(z)$ is the step function equal to $+1$ at positive z and -1 at negative z. Note that B_m^r has discontinuities at $z = 0$ and $z = d$ due to surface currents in the S- and F-films, respectively, whereas the normal component B_m^z is continuous.

A vortex, if appears, must be located at the center of the dot due to symmetry. If $R \gg \lambda$, the direct calculation shows that the central position of the vortex provides minimal energy. For small radius of the dot the deviation of the vortex from the central position seems even less probable. We have checked numerically that central position is always energy favorable for one vortex. Note that this fact is not trivial since the magnetic field of the dot is stronger near its boundary. However, the gain of energy due to interaction of the magnetic field generated by the vortex with magnetization decreases when the vortex approaches the boundary. The normal magnetic field generated by the Pearl vortex is given by equation (22). Numerical calculations based on equations (51, 22) for the case $R > \lambda$ shows that B_z at the S-film ($z = 0$) changes sign at some $r = R_0$ (see figure 2) in the presence of the vortex centered at $r = 0$, but it is negative everywhere at $r > R$ in the absence of the vortex.

The physical explanation of this fact is as follows. The dot itself is an ensemble of parallel magnetic dipoles. Each dipole generates magnetic field at the plane passing through the dot, which has the sign opposite to its dipolar moment. The fields from different dipoles compete at $r < R$, but they have the same sign at $r > R$. The SC current resists this tendency. The field generated by the vortex decays slower than the dipolar field ($1/r^3$ vs. $1/r^4$). Thus, the sign of B_z is opposite to the magnetization at small values of r (but larger than R) and positive at large r. The measurement of magnetic field near the film may serve as a diagnostic tool to detect a S-vortex confined by the dot. To our knowledge, so far there were

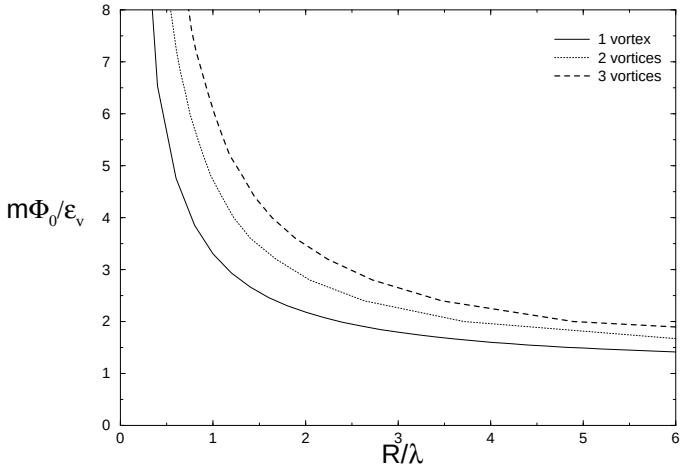

Figure 3: Phase diagram of vortices induced by a magnetic dot. The lines correspond to the appearance of 1,2 and 3 vortices, respectively.

no experimental measurements of this effect.

In the presence of a vortex, energy of the system can be calculated using equations (23-26). The appearance of the vortex changes energy by the amount:

$$\Delta = \varepsilon_v + \varepsilon_{mv} \tag{53}$$

where $\varepsilon_v = \varepsilon_0 \ln(\lambda/\xi)$ is the energy of the vortex without magnetic dot, $\varepsilon_0 = \Phi_0^2/(16\pi^2\lambda)$; ε_{mv} is the energy of interaction between the vortex and the magnetic dot given by equation (26). For this specific problem the direct substitution of the vector-potential, magnetic field and the phase gradient (see equations (50,51))leads to a following result:

$$\varepsilon_{mv} = -m\Phi_0 R \int_0^\infty \frac{J_1(qR)dq}{1+2\lambda q} \tag{54}$$

The vortex appears when Δ turns into zero. This criterion determines a curve in the plane of two dimensional variables R/λ and $m\Phi_0/\varepsilon_v$. This curve separating regimes with and without vortices is depicted in figure 3. The asymptotic of ε_{mv} for large and small values of R/λ can be found analytically:

$$\begin{aligned} \varepsilon_{mv} &\approx - m\Phi_0 \qquad (\frac{R}{\lambda} \gg 1) \\ \varepsilon_{mv} &\approx - m\Phi_0 \frac{R}{2\lambda} \quad (\frac{R}{\lambda} \ll 1) \end{aligned}$$

Thus, asymptotically the curve $\Delta = 0$ turns into a horizontal straight line $m\Phi_0/\varepsilon_v = 1$ at large R/λ and logarithmically distorted hyperbola $(m\Phi_0/\varepsilon_v)(R/\lambda) = 2$ at small ratio R/λ.

At further increasing of either $m\Phi_0/\varepsilon_v$ or R/λ the second vortex becomes energy favorable. Due to symmetry the centers of the two vortices are located on the straight line

including the center of the dot at equal distances from it. The energy of the two-vortex configuration can be calculated by the same method. The curve 2 on figure (3) corresponds to this second phase transition. In principle there exists an infinite series of such transitions. However, here we limit ourselves with the first three since it is not quite clear what is the most energy favorable configuration for 4 vortices (for 3 it is the regular triangle). It is not yet studied what is the role of configurations with several vortices confined inside the dot region and antivortices outside.

3.1.2 Magnetic Dot: Parallel Magnetization

Next we consider an infinitely thin circular magnetic dot whose magnetization $\mathbf{M}$ is directed in the plane and is homogeneous inside the dot. An explicit analytical expression for $\mathbf{M}$ reads as follows:

$$\mathbf{M} = m_0\theta(R-\rho)\delta(z)\hat{x} \tag{55}$$

where R is the radius of the dot, m_0 is the magnetization per unit area and $\hat{x}$ is the unit vector along the x-axis. The Fourier transform of the magnetization is:

$$\mathbf{M_k} = 2\pi m_0 R\frac{J_1(qR)}{q}\hat{x} \tag{56}$$

The Fourier-representation for the vector-potential generated by the dot in the presence of magnetic film takes the form:

$$\begin{aligned}\mathbf{A}^{\perp}_{m\mathbf{k}} &= e^{ikd}[\frac{8\pi^2 m_0 R}{k_z^2+q^2}J_1(qR)cos(\phi_q) \\ &\times \left(\frac{\imath k_z e^{\imath k_z d}}{q} - \frac{e^{-qd}}{1+2\lambda q}\right)]\end{aligned} \tag{57}$$

Let introduce a vortex-antivortex pair with the centers of the vortex and antivortex located at $x=+\rho_0$, $x=-\rho_0$, respectively. Employing equations (23-26) to calculate the energy, we find:

$$\begin{aligned}E &= 2\epsilon_0 ln(\frac{\lambda}{\xi}) - 4\epsilon_0\lambda\int_0^\infty \frac{J_0(2q\rho_0)}{1+2\lambda q}dq \\ &- 2m_0\Phi_0 R\int_0^\infty \frac{J_1(qR)J_1(q\rho_0)}{1+2\lambda q}dq + E_0\end{aligned} \tag{58}$$

where E_0 is the dot self energy. Our numerical calculations indicate that the equilibrium value of ρ_0 is equal to R. The vortex-anti-vortex creation changes the energy of the system by:

$$\begin{aligned}\Delta = 2\epsilon_0 ln(\frac{\lambda}{\xi}) &- 4\epsilon_0\lambda\int_0^\infty \frac{J_0(2qR)}{1+2\lambda q}dq \\ &- 2m_0\Phi_0 R\int_0^\infty \frac{J_1(qR)J_1(qR)}{1+2\lambda q}dq\end{aligned} \tag{59}$$

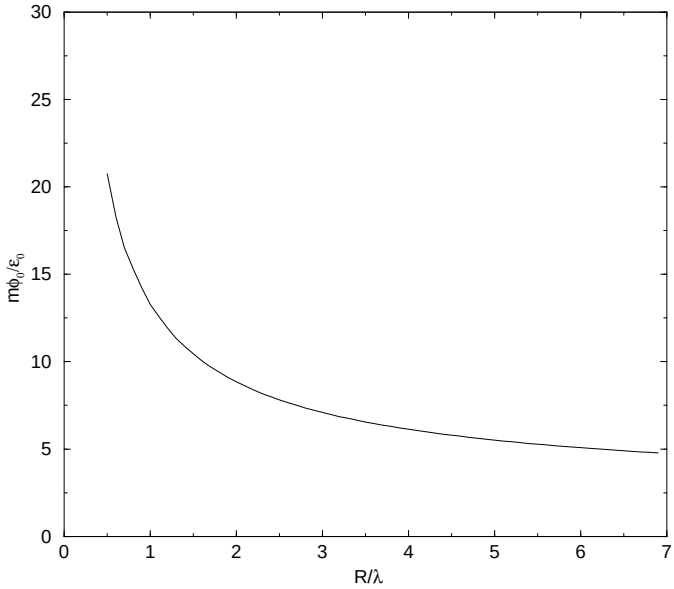

Figure 4: Phase diagram for vortices-anti-vortices induced by the magnetic dot with in-plane magnetization.

The instability to the vortex-anti-vortex pair appearance develops when Δ changes sign. The curve that corresponds to $\Delta = 0$ is given by a following equation:

$$\frac{m_0\Phi_0}{\epsilon_0} = \frac{2ln(\frac{\lambda}{\xi}) - 4\lambda \int_0^\infty \frac{J_0(2qR)}{1+2\lambda q} dq}{2R \int_0^\infty \frac{J_1(qR)J_1(qR)}{1+2\lambda q} dq} \tag{60}$$

The critical curve in the plane of two dimensional ratios $\frac{m_0\Phi_0}{\epsilon_0}$ and $\frac{R}{\lambda}$ is plotted numerically in figure (4). The creation of vortex-anti-vortex is energy unfavorable in the region below this curve and favorable above it. The phase diagram suggests that the smaller is the radius R of the dot the larger value $\frac{m_0\Phi_0}{\epsilon_0}$ is necessary to create the vortex-anti-vortex pair. At large values of R and $m_0\Phi_0 \geq \epsilon_0$, the vortex is separated by a large distance from the antivortex. Therefore, their energy is approximately equal to that of two free vortices. This positive energy is compensated by the attraction of the vortex and antivortex to the magnetic dot. The critical values of $m_0\Phi_0/\epsilon_0$ seems to be numerically large even at $R/\lambda \sim 1$. This is probably a consequence of comparably ineffective interaction of in-plane magnetization with the vortex.

Magnetic dots with a finite thickness were considered by Milosevic *et al.* [42, 43, 44]. No qualitative changes of the phase diagram or magnetic fields were reported.

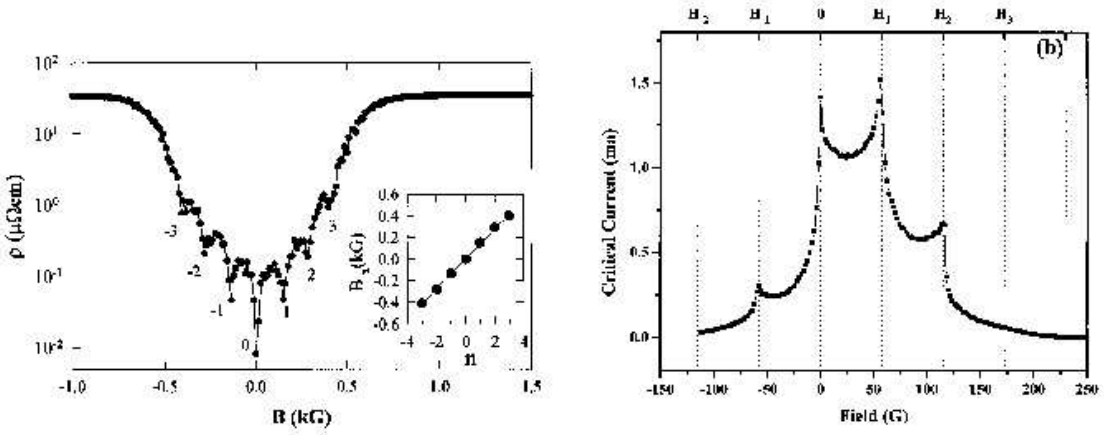

Figure 5: Left: Field dependence of the resistivity of a Nb thin film with a triangular array of Ni dots. (From Martin *et al.* [6]).
Right: Critical current as a function of field for the high density triangular array at T = 8.52 K T_c= 8.56 K (From Morgan and Ketterson [7]).

3.2 Array of Magnetic Dots and Superconducting Film

3.2.1 Vortex Pinning by Magnetic Dots

Vortex pinning in superconductors is of the great practical importance. First time the artificial vortex pinning was created by S-film thickness modulation in seventies. Martinoli *et al.* [10] have used grooves on the film surface to pin vortices and Hebard *et al.* [11, 12] have used triangular arrays of holes. Magnetic structures provide additional possibilities to pin vortices. First experiments were performed in the Louis Neel lab in Grenoble [3, 4]. These experiments were performed with dots several microns wide with the magnetization parallel to the superconducting film. They observed oscillations of the magnetization vs magnetic field. These oscillation was attributed to a simple matching effect: pinning becomes stronger when vortex lattice is commensurate with the lattice of pinning centers. This can be measured in terms of external, normal to the film magnetic field needed to generate integer number of vortices per unit cell of the pinning array.

Flux pinning by a triangular array of submicron size dots with typical spacing 400-600nm and diameters close to 200nm magnetized in-plane was first reported by Martin *et al.* [6]. Oscillations of the resistivity with increasing flux were observed with period corresponding to one flux quanta per unit cell of magnetic dot lattice (see figure 5Left. This can be explained by the matching effect. Though matching effect is not specific to magnetic pinning arrays, enhanced pinning with magnetic dots with magnetization parallel to the film was observed by Martin *et al.* [6].

Dots array with out-of-plane magnetization component was first created and studied by Morgan and Ketterson [7]. They have measured critical current as a function of the external magnetic field and found strong asymmetry of the pinning properties vs magnetic

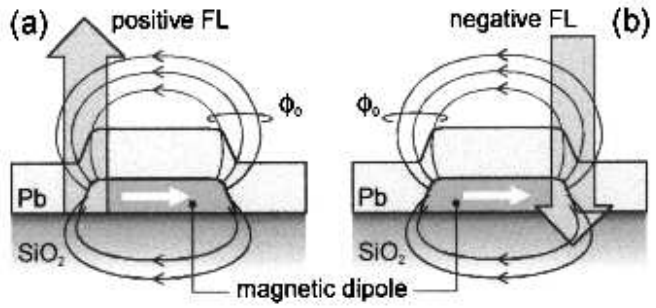

Figure 6: Schematic presentation of the polarity dependent flux pinning, presenting the cross section of a Pb film deposited over a magnetic dipole with in-plane magnetization: (a) A positive FL (wide gray arrow) is attached to the dot at the pole where a negative flux quantum is induced by the stray field (black arrows), and (b) a negative FL is pinned at the pole where a positive flux quantum is induced by the stray field. (From Van Bael *et al.*[87])

field direction (see figure 5Right). This experiment has given the first direct experimental evidence that the physics of vortex pinning by magnetic dots is different from that of common pinning centers.

Pinning properties of the magnetic dots array depends on several factors: magnetic moment orientation, the strength of the stray field, the ratio of the dot size and the dot lattice constant to the effective penetration depth, array magnetization, the strength and direction of the external field, etc. The use of magnetic imaging technique, namely Scanning Hall Probe Microscope (SHPM) and Magnetic Force Microscope (MFM) has revealed exciting pictures of vortex "world". Such studies in combination with traditional measurements gives new insight in vortex physics. This work was done mainly by the group at the University of Leuven. Below we briefly discuss only a few cases studied in great details by this group.

Dots with Parallel Magnetization. Van Bael *et al.*[87] studied with Scanning Hall Probe Microscope (SHPM) the magnetization and vortex distribution in a square array (1.5μm period) of rectangular (540nmX360nm)cobalt trilayer Au(7.5nm)/Co(20nm)/Au(7.5nm) dots with magnetization along the edges of the dots lattice. SHPM images have revealed magnetic field redistribution due to superconducting transition in the covered 50nm thin lead superconducting film. These data were interpreted by Van Bael *et al.*[87] as formation of vortices of opposite sign on both sides of the dot. By applying external magnetic field Van Bael *et al.*[87] have demonstrated the commensurate lattice of vortices residing on the "end" of magnetized dots. This location is in agreement with theoretical prediction [32]. Remarkably, they were able to observe "compensation" of the vortices created by the dots stray field with vortices of the opposite sign due to applied normal field (see figure 6).

Dots with Normal Magnetization. Van Bael *et al.*[88] have elucidated with the SHPM images the nature of previously reported (see e.g. work [7]) anisotropy in the vortices pinning by the array of dots with normal magnetization. They have used 1μm period lattice of square, 400nm side length and 14nm thin, Co/Pt multilayer dots covered with 50nm thin lead film.

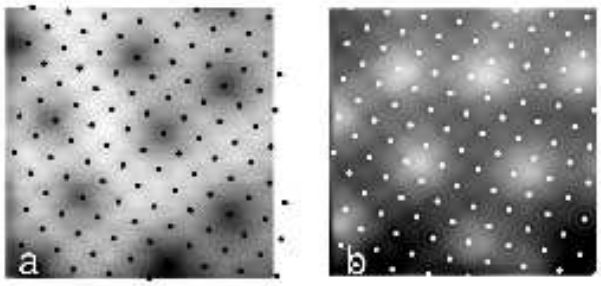

Figure 7: SHPM images of a $(10.5\mu\text{m})^2$ area of the sample in H=-1.6 Oe (left panel) and H=1.6 Oe (right panel), at T=6.8 K (field-cooled). The tiny black/white dots indicate the posi- tions of the Co/Pt dots, which are all aligned in the negative sense (m < 0). The flux lines emerge as diffuse dark (H < 0) or bright (H > 0) spots in the SHPM images. (From Van Bael *et al.*[88])

Zero field SHPM images show the checkerboard-like distribution of magnetic field (see Sec. 3.3.4) The stray field from the dots were not sufficient to create vortices. In a very weak (1.6 Oe) external field the average distance between vortices was about 4 lattice spacings. In the case of the field parallel to the dots magnetization vortices reside on the dots, as the SHPM image shows (see figure 7a). In the case of the same field with opposite direction, the SHPM shows vortices located at interstitial positions in the magnetic dots lattice (see figure 7b). It is plausible that the pinning barriers are lower in the second case.

Figure 8 shows dependance of superconduction film magnetization versus applied magnetic field normal to the film. Moshchalkov *et al.*[89] have shown that magnetic field dependence of film magnetization of the superconducting film is very similar to the critical current dependence on magnetic field. Figure 8 shows strong anisotropy of the pinning properties on the external magnetic field direction. Magnetic field parallel to the dots magnetic moment shows much stronger vortex pinning than antiparallel.

3.2.2 Magnetic Field Induced Superconductivity

Consider a regular array of magnetic dots placed upon a superconducting film with magnetization normal to the film. For simplicity we consider very thin magnetic dots. Namely this situation is realized magnetic films with normal magnetization used in experiment [90]). The net flux from the magnetic dot through any plane including the surface of the superconducting film (see figure 9) is exactly zero. Suppose that on the top of the magnetic dot the z-component of the magnetic field is positive as shown in the mentioned figure. Due to the requirement of zero net flux the z-component of the magnetic field between the dots must be negative. Thus, S-film occurs in a negative magnetic field normal to the film. It can be partly or fully compensated by an external magnetic field parallel to the dot magnetization (see figure 9). Such a compensation can be even more effective in for a regular array of

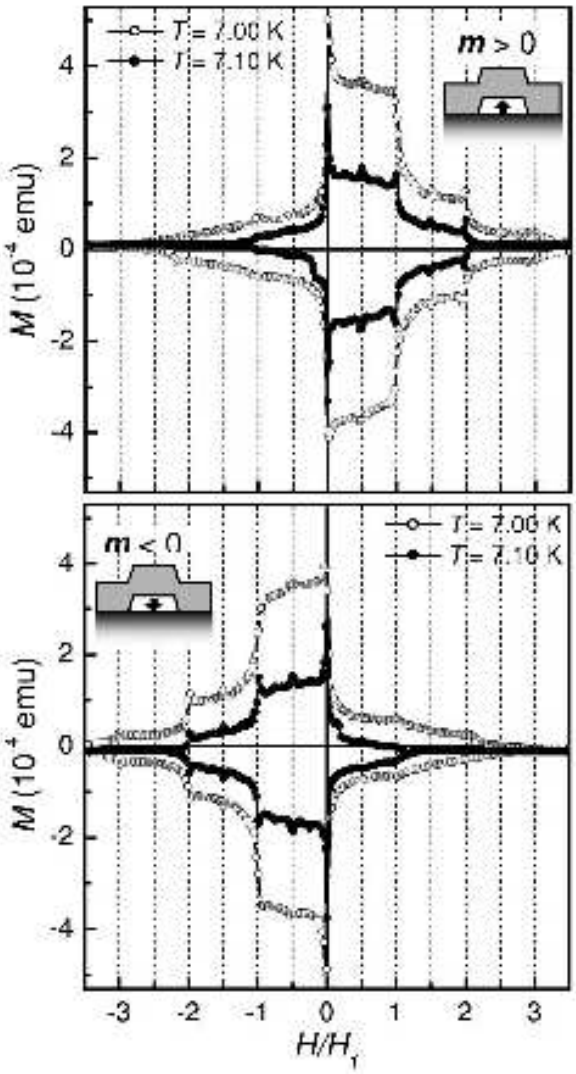

Figure 8: M (H/H_1) magnetization curves at different temperatures near T_c (7.00 K open symbols, 7.10 K filled symbols) showing the superconducting response of the Pb layer on top of the Co/Pt dot array with all dots aligned in a positive upper panel and negative lower panel sense. H_1=20.68 Oe is the first matching field. (From Van Bael *et al.*[88])

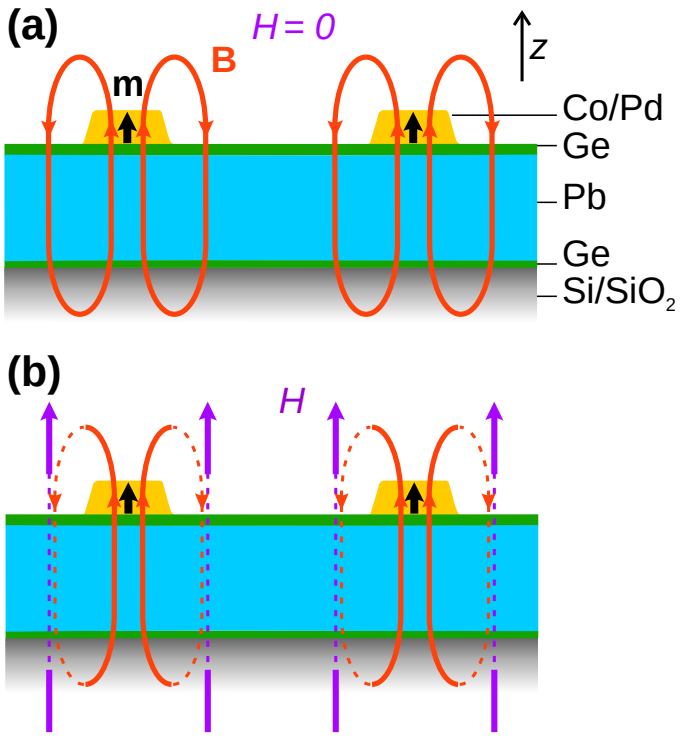

Figure 9: Schematical magnetic field distribution in the the array of dots with normal to the superconducting film magnetization. (From Lange *et al.* cond-mat/0209101)

magnetic wires embedded in alumina template [35, 37, 91]. Lange *et al.*[90] have proposed this trick and reached a positive shift of the S-transition temperature in an external magnetic field, the result looking counterintuitive if one forgets about the field generated by the dots. In this experiment a thin superconducting film was covered with a square array of the CoPd magnetic dots with normal to the film magnetization. The dots had square shape with the side 0.8μm, the thickness 22nm and the dot array period 1.5μm. The H-T phase diagrams presented in [90] for zero and finite dots magnetization demonstrate appearance of the superconductivity by applying magnetic field parallel to the dot magnetization. At T=7.20K the system with magnetized dots is in normal state. It undergoes transition to the superconducting state in the field 0.6mT and back to the normal state at 3.3mT. From the data in figure 3 in work by Lange *et al.*[90] one can conclude that the compensating field is about 2mT.

3.2.3 Magnetization Controlled Superconductivity

Above (Sec. 3.2.2) we have discussed example when application of magnetic field can transform FSH system from normal to superconducting state. This was due compensation of the dots stray magnetic field with external magnetic field.

Earlier Lyuksyutov and Pokrovsky [26] have discussed theoretically situation when de-

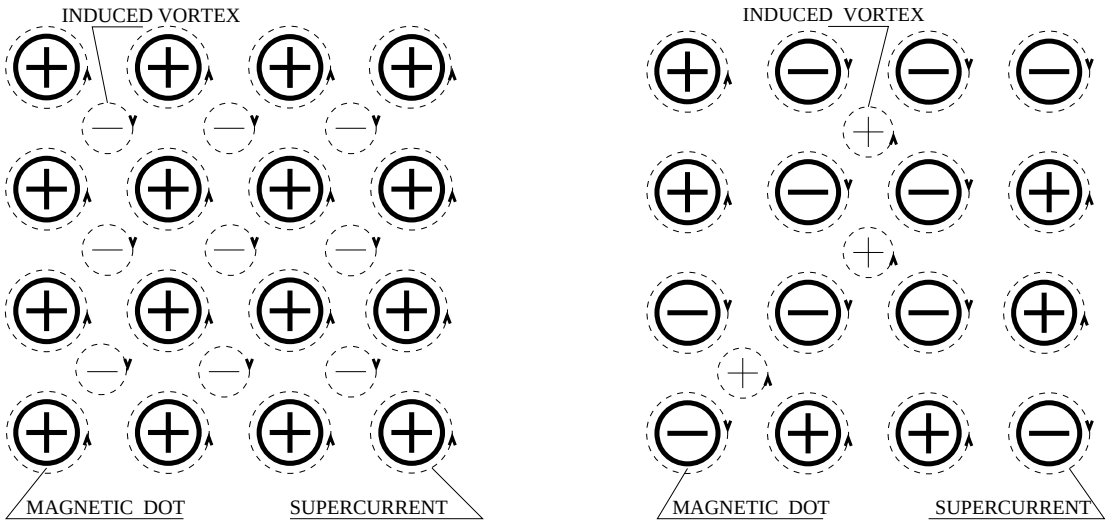

Figure 10: Left: Magnetized magnetic dots array. Vortices of different signs are shown schematically by supercurrent direction (dashed lines). The magnetic moment direction is indicated by $\pm$. Both vortices bound by dots and created spontaneously are shown. Magnetized array of dots create regular lattice of vortices and antivortices and provide strong pinning. Right: Demagnetized magnetic dots array results in strongly fluctuating random potential which creates unbound antivortices/vortices, thus transforming superconducting film into resistive state.

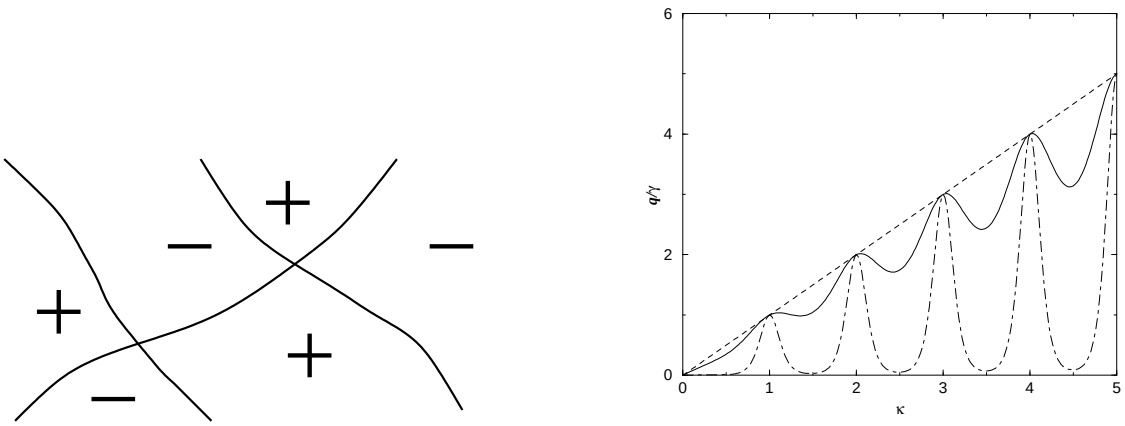

Figure 11: Left:The checker-board average structure of the vortex plasma. Right: The average number of the unbound vortices in the cell of size a via the parameter κ proportional to the dot magnetic moment. Dot-dashed line corresponds to $T/\epsilon_0 = 0.15$, solid line corresponds to $T/\epsilon_0 = 0.4$, dashed line corresponds to $T/\epsilon_0 = 2$.

magnetized array of magnetic dots with normal magnetization create resistive state in the coupled superconducting film. However, superconducting state can be restored by magnetization of the dots array. This counter intuitive phenomena can be explained on qualitative level. In the case when single dot creates one vortex, magnetized array of dots results in periodical vortex/antivortex structure with anti-vortices localized at the centers of the unit cells of the square lattice of dots as shown in figure 10Left. Such order provides strong pinning. More interesting is demagnetized state in which the induced vortices and antivortices create a random field for a probe vortex. If the lattice constant of the array a is less than the effective penetration depth λ, the random fields from vortices are logarithmic. The effective number of random logarithmic potentials acting on a probe vortex is $N = (\lambda/a)^2$ and the effective depth of potential well for a vortex (antivortex) is $\sqrt{N}\epsilon_v$. At proper conditions, for example near the S-transition point, the potential wells can be very deep enabling the spontaneous generation of the vortex-antivortex pairs at the edges between potential valleys and hills. The vortices and antivortices will screen these deep wells and hills similarly to the screening in the plasma. The difference is that, in contrast to plasma, the screening "charges" do not exist without external potential. In such a flattened self-consistent potential relief the vortices have percolated infinite trajectories passing through the saddle points [29]. The drift motion of the delocalized vortices and antivortices in the external field generates dissipation and transfer the S-film into the resistive state (see figure 10Right). Replacing slow varying logarithmic potential by a constant at distances less than λ and zero at larger distances, Feldman *et al.* have found thermodynamic and transport characteristics of this system. Below we briefly outline their main results. For the sake of simplicity we replace this slow varying potential $V(\mathbf{r})$ by a potential having a constant value within the single cell: $V_0 = 2\epsilon_0$ at the distance $r < \lambda$ and zero at $r > \lambda$, where $\epsilon_0 = \Phi_0^2/(16\pi^2\lambda)$, Φ_0

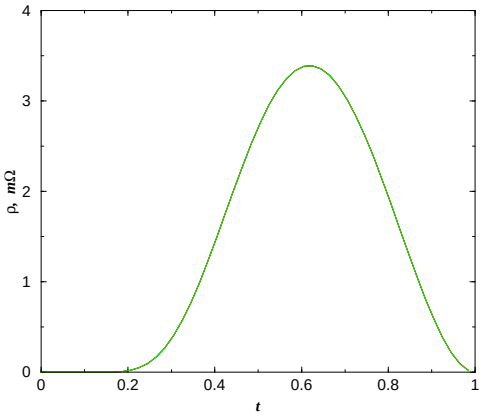

Figure 12: The static resistance ρ of the film vs dimensionless temperature $t = T/T_c$ at typical values of parameters.

is the magnetic flux quantum. Considering the film as a set of almost unbound cells of the linear size λ we arrive at the following Hamiltonian for such a cell:

$$H = -U \sum_i \sigma_i n_i + \epsilon \sum_i n_i^2 + 2\epsilon_0 \sum_{i>j} n_i n_j, \tag{61}$$

where n_i is integer vorticity on either a dot and or a site of the dual lattice (between the dots) which we conventionally associate with location of unbound vortices. $\sigma_i = \pm 1$, where subscript i relates to the dot, describes the random sign of the dot magnetic moments. $\sigma_i = 0$ on the sites of dual lattice. The first term of the Hamiltonian (61) describes the binding energy of the vortex at the magnetic dot and $U \approx \epsilon_0 \Phi_d/\Phi_0$, with Φ_d being the magnetic flux through a single dot. The second term in the Hamiltonian is the sum of single vortex energies, $\epsilon = \epsilon_0 \ln(\lambda_{\rm eff}/a)$, where a is the period of the dot array, ξ is the superconducting coherence length. The third term mimics the intervortex interaction. Redefining the constant ϵ, one can replace the last term of equation (61) by $\epsilon_0(\sum n_i)^2$. The sign of the vorticity on a dot follows two possible ('up'- and 'down-') orientations of its magnetization. The vortices located between the dots (n_i on the dual lattice) are correlated on the scales of order λ and form the above-mentioned irregular checker-board potential relief.

To find the ground state, we consider a cell with large number of the dots of each sign $\sim (\lambda/a)^2 \gg 1$. The energy (61) is minimal when the "neutrality" condition $Q \equiv \sum n_i = 0$ is satisfied. Indeed, if $Q \neq 0$ the interaction energy grows as Q^2, whereas the first term of the Hamiltonian behaves as $|Q|$ and can not compensate the last one unless $Q \sim 1$. The neutrality constraint means that the unbound vortices screen almost completely the "charge" of those bound by dots, that is $K \sim (N_+ - N_-) \sim \sqrt{N_\pm} \sim \lambda/a$ where K is the difference between the numbers of the positive and negative dots and $N_\pm$ are the numbers of the positive and negative vortices, respectively. Neglecting the total charge $|Q|$ as compared with λ/a, we minimize the energy (61) accounting for the neutrality constraint. At $Q = 0$

the Hamiltonian (61) can be written as the sum of one-vortex energies:

$$H = \sum H_i; \qquad H_i = -U\sigma_i n_i + \epsilon n_i^2. \tag{62}$$

The minima for any H_i is achieved by choosing $n_i = n_i^0$, an integer closest to the magnitude $\sigma_i\kappa = \sigma_i U/(2\epsilon)$. The global minimum consistent with the neutrality is realized by values of n_i that differ from the local minima values n_i^0 not more than over ± 1. Indeed, in the configuration with $n_i = n_i^0$, the total charge is $|\sum n_i^0| \sim \kappa|\sum \sigma_i| = \kappa K$. Hence, if $\kappa \ll \lambda/a$, then the change of the vorticity at a small part of sites by ± 1 restores neutrality. To be more specific let us consider $K > 0$. Let $\bar{n}$ be the integer closest to κ, and consider the case $\kappa < \bar{n}$. Then the minimal energy corresponds to a configuration with the vorticity $n_i = -\bar{n}$ at each negative dot and with the vorticity $\bar{n}$ or $\bar{n} - 1$ at positive dots. The neutrality constraint implies that the number of positive dots with the vorticity $\bar{n}-1$ is $M = K\bar{n}$. In the opposite case $\kappa > \bar{n}$ the occupancies of all the positive dots are $\bar{n}$; whereas, the occupancies of the negative dots are either $\bar{n}$ or $\bar{n}+1$. Note that in our model the unbound vortices are absent in the ground state unless κ is an integer. Indeed, the transfer of a vortex from a dot with the occupancy n to a dual site changes the energy by $\Delta E = 2\epsilon(\kappa - n + 2)$. Hence, the energy transfer is zero if and only if κ is an integer, otherwise the energy change upon the vortex transfer is positive. At integer κ, the number of the unbound vortices can vary from 0 to $K\bar{n}$ without change of energy. The ground state is degenerate at any non-integer κ since, while the total number of the dots with the different vorticities are fixed, the vortex exchange between two dots with the vorticities n and $n \pm 1$ does not change the total energy. Thus, our model predicts a step-like dependence of dot occupancies on κ at the zero temperature and peaks in the concentration of unbound vortices as shown in figure 11. The data for finite temperature were calculated in the Ref.[29] The dependencies of the unbound vortex concentration on κ for several values of $x = \epsilon/T$ are shown in figure 11. Oscillations are well pronounced for $x \gg 1$ and are suppressed at small x (large temperatures). At low temperatures, $x \gg 1$, the half-widths of the peaks in the density of the unbound vortices are $\Delta\kappa \approx 1/x$ and the heights of peaks are $\approx \gamma n$, where $\gamma = K/N$.

Vortex transport– At moderate external currents j the vortex transport and dissipation are controlled by unbound vortices. The typical energy barrier associated with the vortex motion is ϵ_0. The unbound vortex density is $m \sim a^{-2}\gamma \sim (a\lambda)^{-1}$ and oscillates with κ as it was shown above. The average distance between the unbound vortices is $l \sim \sqrt{a\lambda}$. The transport current exerts the Magnus (Lorentz) force $F_M = j\Phi_0/c$ acting on a vortex. Since the condition $T \ll \epsilon_0$ is satisfied in the vortex state everywhere except for the regions too close to T_c, the vortex motion occurs via thermally activated jumps with the rate:

$$\nu = \nu_0 \exp(-\epsilon_0/T) = (\mu j \Phi_0/cl) \exp(-\epsilon_0/T), \tag{63}$$

where $\mu = (\xi^2\sigma_n)/(4\pi e^2)$ is the Bardeen-Stephen vortex mobility [92]. The induced electric field is accordingly

$$E_c = l\dot{B}/c = m\Phi_0\nu l/c, \tag{64}$$

The Ohmic losses per unbound vortex are $W_c = jE_c\lambda a = j\Phi_0\nu l/c$ giving rise to the dc resistivity as

$$\rho_{\rm dc} = \frac{W_c}{j^2\lambda^2} = \frac{\mu\Phi_0^2}{c^2\lambda^2}\exp[-\epsilon_0(T)/T] \tag{65}$$

Note the non-monotonic dependence of $\rho_{\rm dc}$ on temperature T figure 12. The density of the unbound vortices is the oscillating function of the flux through a dot. The resistivity of such a system is determined by thermally activated jumps of vortices through the corners of the irregular checkerboard formed by the positive or negative unbound vortices and oscillates with Φ_d. These oscillations can be observed by additional deposition (or removal) of the magnetic material to the dots.

3.3 Ferromagnet - Superconductor Bilayer

3.3.1 Topological Instability in the FSB

Let us consider a F/S bilayer with both layers infinite and homogeneous. An infinite magnetic film with ideal parallel surfaces and homogeneous magnetization generates no magnetic field outside. Indeed, it can be considered as a magnetic capacitor, the magnetic analog of an electric capacitor, and therefore its magnetic field confined inside. Thus, there is no direct interaction between the homogeneously magnetized F-layer and a homogeneous S-layer in the absence of currents in it. However, Lyuksyutov and Pokrovsky argued [30] that such a system is unstable with respect to spontaneous formation of vortices in the S-layer. Below we reproduce these arguments.

Assume the magnetic anisotropy to be sufficiently strong to keep magnetization perpendicular to the film (in the z-direction). As we have demonstrated above, the homogeneous F-film creates no magnetic field outside itself. However, if a Pearl vortex somehow appears in the superconducting film, it generates magnetic field interacting with the magnetization $\mathbf{m}$ per unit area of the F-film. At a proper circulation direction in the vortex and the rigid magnetization $\mathbf{m}$ this field decreases the total energy over the amount $m\int B_z(\mathbf{r})d^2x = m\Phi$, where Φ is the total flux. We remind that each Pearl vortex carries the flux equal to the famous flux quantum $\Phi_0 = \pi\hbar c/e$. The energy necessary to create the Pearl vortex in the isolated S-film is $\epsilon_v^{(0)} = \epsilon_0\ln(\lambda/\xi)$ [72], where $\epsilon_0 = \Phi_0^2/16\pi^2\lambda$, $\lambda = \lambda_L^2/d$ is the effective penetration depth[71], λ_L is the London penetration depth, and ξ is the coherence length. Thus, the total energy of a single vortex in the FSB is:

$$\epsilon_v = \epsilon_v^{(0)} - m\Phi_0, \tag{66}$$

and the FSB becomes unstable with respect to spontaneous formation vortices as soon as ϵ_v turns negative. Note that close enough to the S-transition temperature T_s, ϵ_v is definitely negative since the S-electron density n_s and, therefore, $\epsilon_v^{(0)}$ is zero at T_s. If m is so small that $\epsilon_v > 0$ at $T = 0$, the instability exists in a temperature interval $T_v < T < T_s$, where T_v is defined by equation $\epsilon_v(T_v) = 0$. Otherwise instability persists till $T = 0$.

A newly appearing vortex phase cannot consist of the vortices of one sign. More accurate statement is that any finite, independent on the size of the film L_f density of vortices is

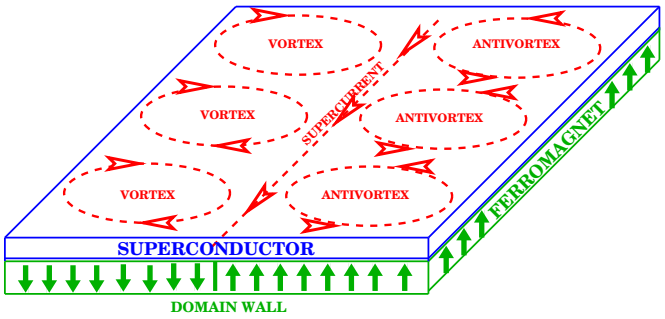

Figure 13: Magnetic domain wall and coupled arrays of superconducting vortices with opposite vorticity. Arrows show the direction of the supercurrent.

energetically unfavorable in the thermodynamic limit $L_f \to \infty$. Indeed, any system with the non-zero average vortex density n_v generates a constant magnetic field $B_z = n_v \Phi_0$ along the z direction. The energy of this field for a large but finite film of the linear size L_f grows as L_f^3 exceeding the gain in energy due to creation of vortices proportional to L_f^2 in thermodynamic limit. Thus, paradoxically the vortices appear, but can not proliferate to a finite density. This is a manifestation of the long-range character of magnetic forces. The way from this controversy is similar to that in ferromagnet: the film should split in domains with alternating magnetization and vortex circulation directions. Note that these are combined topological defects: vortices in the S-layer and domain walls in the F-layer. They attract each other. The vortex density is higher near the domain walls. The described texture represents a new class of topological defects which does not appear in isolated S and F layers. We show below that if the domain linear size L is much greater than the effective penetration length λ, the most favorable arrangement is the stripe domain structure (see (figure 13)). The quantitative theory of this structure was given by Erdin *et al.* [31].

The total energy of the bilayer can be represented by a sum:

$$U = U_{sv} + U_{vv} + U_{vm} + U_{mm} + U_{dw} \tag{67}$$

where U_{sv} is the sum of energies of single vortices; U_{vv} is the vortex-vortex interaction energy; U_{vm} is the energy of interaction between the vortices and magnetic field generated by domain walls; U_{mm} is the self-interaction energy of magnetic layer; U_{dw} is the linear tension energy of domain walls. We assume the 2d periodic domain structure consisting of two equivalent sublattices. The magnetization $m_z(\mathbf{r})$ and density of vortices $n(\mathbf{r})$ alternate when passing from one sublattice to another. Magnetization is supposed to have a constant absolute value: $m_z(\mathbf{r}) = ms(\mathbf{r})$, where $s(\mathbf{r})$ is the periodic step function equal to +1 at one sublattice and -1 at the other one. We consider a dilute vortex system in which the vortex spacing is much larger than λ. Then the single-vortex energy is:

$$U_{sv} = \epsilon_v \int n(\mathbf{r}) s(\mathbf{r}) d^2x; \quad \epsilon_v = \epsilon_v^{(0)} - m\Phi_0 \tag{68}$$

The vortex-vortex interaction energy is:

$$U_{vv} \;=\; \frac{1}{2}\int n(\mathbf{r})V(\mathbf{r}-\mathbf{r}')n(\mathbf{r}')d^2xd^2x', \tag{69}$$

where $V(\mathbf{r}-\mathbf{r}')$ is the pair interaction energy between vortices located at points $\mathbf{r}$ and $\mathbf{r}'$. Its asymptotics at large distances $\mid \mathbf{r}-\mathbf{r}' \mid \gg \lambda$ is $V(\mathbf{r}-\mathbf{r}') = \Phi_0^2/(4\pi^2 \mid \mathbf{r}-\mathbf{r}' \mid)$ [93]. This long-range interaction is induced by magnetic field generated by the Pearl vortices and their slowly decaying currents[3]. The energy of vortex interaction with the magnetic field generated by the magnetic film looks as follows [32]:

$$U_{vm} \;=\; -\frac{\Phi_0}{8\pi^2\lambda}\int \nabla\varphi(\mathbf{r}-\mathbf{r}')n(\mathbf{r}')\cdot\mathbf{a}^{(m)}(\mathbf{r})d^2xd^2x' \tag{70}$$

Here $\varphi(\mathbf{r}-\mathbf{r}') = \arctan\frac{y-y'}{x-x'}$ is a phase shift created at a point $\mathbf{r}$ by a vortex centered at a point $\mathbf{r}'$ and $\mathbf{a}^{(m)}(\mathbf{r})$ is the value of the vector-potential induced by the F-film upon the S-film. This part of energy similarly to what we did for one vortex can be reduced to the renormalization of the single vortex energy with the final result already shown in equation (68). The magnetic self-interaction reads:

$$U_{mm} \;=\; -\frac{m}{2}\int B_z^{(m)}(\mathbf{r})s(\mathbf{r})d^2x \tag{71}$$

Finally, the domain walls linear energy is $U_{dw} = \epsilon_{dw}L_{dw}$ where ϵ_{dw} is the linear tension of the domain wall and L_{dw} is the total length of the domain walls.

Erdin *et al.*[31] have compared energies of stripe, square and triangular domain wall lattices, and found that stripe structure has the lowest energy. Details of calculation can be found in [31] (see correction in [33]. The equilibrium domain width and the equilibrium energy for the stripe structure are:

$$L_s = \frac{\lambda}{4}\exp\left(\frac{\varepsilon_{dw}}{4\tilde{m}^2} - C + 1\right) \tag{72}$$

$$U_s = -\frac{16\widetilde{m}^2}{\lambda}\exp\left(-\frac{\varepsilon_{dw}}{4\widetilde{m}^2} + C - 1\right) \tag{73}$$

where $\tilde{m} = m - \epsilon_v^0/\Phi_0$ and C=0.57721 is the Euler constant.The vortex density for the stripe domain case is:

$$n(x) \;=\; -\frac{4\pi\tilde{\epsilon}_v}{\Phi_0^2 L_s}\frac{1}{\sin(\pi x/L_s)} \tag{74}$$

Note a strong singularity of the vortex density near the domain walls. Our approximation is invalid at distances of the order of λ, and the singularities must be smeared out in the band of the width λ around the domain wall.

[3]From this long-range interaction of the Pearl vortices it is ready to derive that the energy of a system of vortices with the same circulation, located with the permanent density n_v on a film having the lateral size L, is proportional to $n_v^2L^3$

The domains become infinitely wide at $T = T_s$ and at $T = T_v$. If $\epsilon_{dw} \leq 4\tilde{m}^2$, the continuous approximation becomes invalid (see sec. 3.2.3) and instead a discrete lattice of vortices must be considered. It is possible that the long nucleation time can interfere with the observation of described textures. We expect, however that the vortices that appear first will reduce the barriers for domain walls and, subsequently, expedite domain nucleation.

Despite of theoretical simplicity the ideal bilayer is not easy to realize experimentally. The most popular material with the perpendicular to film magnetization is a multilayerer made from Co and Pt ultrathin films (see Sec.3.3.4). This material has very large coercive field and rather chaotic morphology. Therefore, the domain walls in such a multilayer are chaotic and almost unmovable at low temperatures (see Sec.3.3.4). We hope, however, that these experimental difficulties will be overcome and spontaneous vortex structures will be discovered before long.

3.3.2 Superconducting transition temperature of the FSB

The superconducting phase transition in ferromagnet-superconductor bilayer was studied by Pokrovsky and Wei [33]. They have demonstrated that in the FSB the transition proceeds discontinuously as a result of competition between the stripe domain structure in a FM layer at suppressed superconductivity and the combined vortex-domain structure in the FSB. Spontaneous vortex-domain structures in the FSB tend to increase the transition temperature, whereas the effect of the FM self-interaction decreases it. The final shift of transition temperature T_c depends on several parameters characterizing the SC and FM films and varies typically between -0.03T_c and 0.03T_c .

As it was discussed earlier, the homogeneous state of the FSB with the magnetization perpendicular to the layer is unstable with respect to formation of a stripe domain structure, in which both, the direction of the magnetization in the FM film and the circulation of the vortices in the SC film alternate together. The energy of the stripe structure per unit area U and the stripe equilibrium width L_s is given in equations 73, 72. To find the transition temperature, we combine the energy given by equation 73 with the Ginzburg-Landau free energy. The total free energy per unit area reads:

$$F = U + F_{GL} = \frac{-16\tilde{m}^2}{\lambda_e} \exp(\frac{-\epsilon_{dw}}{4\tilde{m}^2} + C - 1) + n_s d_s[\alpha(T - T_c) + \frac{\beta}{2} n_s] \,. \tag{75}$$

Here α and β are the Ginzburg-Landau parameters. We omit the gradient term in the Ginzburg-Landau equation since the gradients of the phase are included in the energy (73), whereas the gradients of the superconducting electrons density can be neglected everywhere beyond the vortex cores. Minimizing the total free energy Pokrovsky and Wei [33] have found that near T_c the FSB free energy can be represented as

$$F_s = -\frac{\alpha^2 (T - T_r)^2}{2\beta} d_s \tag{76}$$

where T_r is given by the equation:

$$T_r = T_c + \frac{64\pi m^2 e^2}{\alpha m_s c^2} \exp(\frac{-\epsilon_{dw}}{4m^2} + C - 1) \tag{77}$$

The SC phase is stable if its free energy equation 76 is less than the free energy of a single FM film with the stripe domain structure, which has the following form [94, 95]:

$$F_m = -\frac{4m^2}{L_f} \tag{78}$$

where L_f is the stripe width of the single FM film. Near the SC transition point the temperature dependence of the variation of this magnetic energy is negligible. Hence, when T increases, the SC film transforms into a normal state at some temperature T_c^* below T_r. This is the first-order phase transition. At transition point both energies F_s and F_m are equal to each other. The shift of the transition temperature is determined by a following equation:

$$\Delta T_c \equiv T_c^* - T_c = \frac{64\pi m^2 e^2}{\alpha m_s c^2} \exp(\frac{-\epsilon_{dw}}{4m^2} + C - 1) - \sqrt{\frac{8\beta m^2}{\alpha^2 d_s L_f}} \tag{79}$$

Two terms in equation 79 play opposite roles. The first one is due to the appearance of spontaneous vortices which lowers the free energy of the system and tends to increase the transition temperature. The second term is the contribution of the purely magnetic energy, which tends to decrease the transition temperature. The values of parameters entering equation 79 can be estimated as follows. The dimensionless Ginzburg-Landau parameter is $\alpha = 7.04 T_c/\epsilon_F$, where ϵ_F is the Fermi energy. A typical value of α is about 10^{-3} for low-temperature superconductors. The second Ginzburg-Landau parameter is $\beta = \alpha T_c/n_e$, where n_e is the electron density. For estimates Pokrovsky and Wei [33] take $T_c \sim 3$K, $n_e \sim 10^{23}$ cm^3. The magnetization per unit area m is the product of the magnetization per unit volume M and the thickness of the FM film d_m. For typical values of $M \sim 10^2$ Oe and $d_m \sim 10$nm. $m \sim 10^{-4}$ Gs/cm^2. In an ultrathin magnetic film the observed values of L_f vary in the range 1 to 100μm [96, 97]. If $L_f \sim 1\mu$m, $d_s = d_m = 10$nm, and $\exp(-\tilde{\epsilon}_{dw}/4m^2 + C - 1) \approx 10^{-3}$, $\Delta T_c/T_c \sim -0.03$. For $L_f = 100\mu$m, $d_s = 50$nm, and and $\exp(-\tilde{\epsilon}_{dw}/4m^2 + C - 1) \approx 10^{-2}$, $\Delta T_c/T_c \sim 0.02$.

3.3.3 Transport properties of the FSB

The spontaneous domain structure violates initial rotational symmetry of the FSB. Therefore, it makes transport properties of the FSB anisotropic. Kayali and Pokrovsky [34] have calculated the periodic pinning force in the stripe vortex structure resulting from a highly inhomogeneous distribution of the vortices and antivortices in the FSB. The transport properties of the FSB are associated with the driving force acting on the vortex lattice from an external electric current. In the FSB the pinning force is due to the interaction of the domain

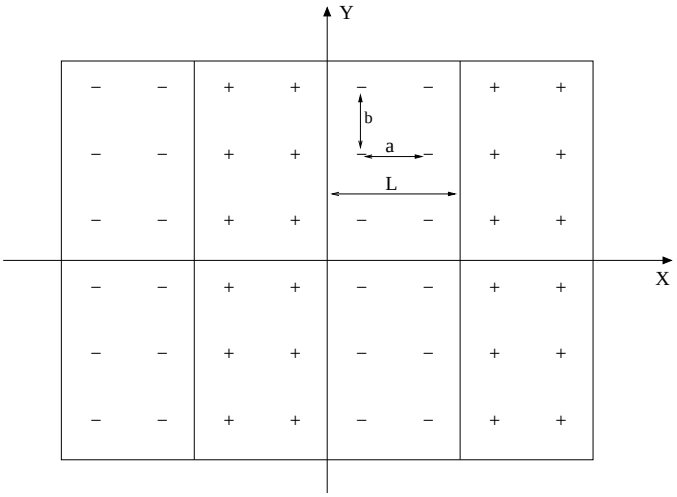

Figure 14: Schematic vortex distribution in the FSB. The sign ± refers to the vorticity of the trapped flux.

walls with the vortices and antivortices and the vortex-vortex interaction U_{vv} Periodic pinning forces in the direction parallel to the stripes do not appear in continuously distributed vortices. In the work [34] the discreteness effects were incorporated. Therefore, one need to modify the theory [31] to incorporate the discreteness effects.

Kayali and Pokrovsky [34] have showed that, in the absence of a driving force, the vortices and antivortices lines themselves up in straight chains and that the force between two chains of vortices falls off exponentially as a function of the distance separating the chains. They also argued that pinning force in the direction parallel to the domains drops faster in the vicinity of the superconducting transition temperature T_s and vortex disappearance temperature T_v.

In the presence of a permanent current there are three kinds of forces acting onto a vortex. They are i) The Magnus force proportional to the vector product of the current density and the velocity of the vortex; ii) The viscous force directed oppositely to the vortex velocity; iii) Periodic pinning force acting on a vortex from other vortices and domain walls. The pinning force have perpendicular and parallel to domain walls components. In the continuous limit the parallel component obviously vanishes. It means that it is exponentially small if the distances between vortices are much less than the domain wall width. The sum of all three forces must be zero. This equation determines the dynamics of the vortices. It was solved under a simplifying assumptions that vortices inside one domain move with the same velocity. The critical current have been calculated for for parallel and perpendicular orientation. Theory predicts a strong anisotropy of the critical current. The ratio of the parallel to perpendicular critical current is expected to be in the range $10^2 \div 10^4$ close to the superconducting transition temperature T_s and to the vortex disappearance temperature T_v. The anisotropy decreases rapidly when the temperature goes from the ends of this interval reaching its minimum somewhere inside it. The anisotropy is associated with the fact that the motion of vortices is very different in this two cases. At perpendicular to the domains

direction of the permanent current all the vortices are involved by the friction force into a drift in the direction of the current, whereas the Magnus force induces the motion of vortices (antivortices) in neighboring domains in opposite directions, both perpendicular to the current. The motion of all vortices perpendicular to the domains captures domain walls, which also move in the same direction. This is a Goldstone mode, no perpendicular pinning force appears in this case. The periodic pinning in the parallel direction and together with it the perpendicular critical current is exponentially small. In the case of parallel current the viscous force involves all vortices into the parallel motion along the domain walls and in alternating motion perpendicularly to them. The domain walls remain unmoving and provide very strong periodic pinning force in the perpendicular direction. This anisotropic transport behavior could serve as a diagnostic tool to discover spontaneous topological structures in magnetic-superconducting systems.

3.3.4 Experimental studies of the FSB

In the preceding theoretical discussion we assumed that the magnetic film changes its magnetization direction in a weak external field and achieves the equilibrium state. All experimental works have been done with the Co/Pt, Co/Pd multilayers, which have large coercive field and are virtually "frozen" at the experiment temperature. Lange *et al.* [98, 99, 100] have studied phase diagram and pinning properties of such magnetically "frozen" FSB. In these works the average magnetization is characterized by the parameter s, the fraction of spins directed up. Magnetic domains in Co/Pd(Pt) multilayers look like meandering irregular bands at $s = 0.5$ (zero magnetization) (see figure 15b) and as "bubble" domains (see figure 15d) with typical size 0.25μm-0.35μm near fully magnetized states ($s = 0$ or $s = 1$). The stray field from domains is maximal at $s = 0.5$ and decreases the superconducting transition temperature T_c of the Pb film by 0.2K (see figure 16). The effective penetration depth is about 0.76μm at 6.9K.

Close to $s = 0$ or $s = 1$ Lange *et al.* [98, 99, 100] have observed behavior in the applied magnetic field which is similar to the array of magnetic dots with normal to the film magnetization (see Sec. 3.2.1). They have found asymmetry in the applied magnetic field for $T_c(H)$ dependence and for pinning properties. The bubble domains have a perpendicular magnetic moment. If the thickness and magnetization is sufficient, they can pin vortices which appear in the applied external magnetic field. In this respect they are similar to randomly distributed dots with normal magnetization. Thus, in the range of filling factor $s \approx 0\,\text{or}1$ the critical current must be large enough. Contrary to this situation at $s \approx 0.5$ the randomly bent band domains destroy a possible order of the vortex lattice and provide percolation "routes" for the vortex motion. Thus the pinning is weaker and corresponds either to smaller critical current or to a resistive state. This qualitative difference between magnetized and demagnetized state has been observed in the experiments by Lange et al([98, 99, 100]). The above qualitative picture of vortex pinning is close to that developed by Lyuksyutov and Pokrovsky [26] and by Feldman et al [29] for the transport properties of the regular array of magnetic dots with the random normal magnetization (see Sec.3.2.3). In this model the demagnetized state of the dot array is associated with the vortex creep

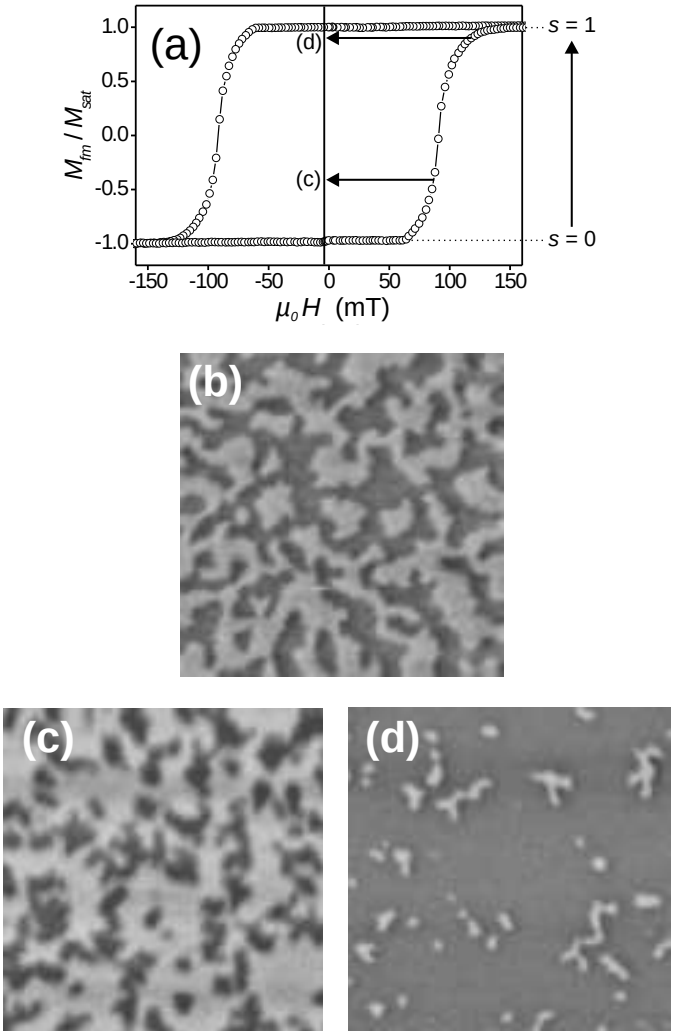

Figure 15: Magnetic properties of the Co/Pt multilayer: (a) Hysteresis loop measured by magneto-optical Kerr effect with H perpendicular to the sample surface. MFM images (5×5 μm^2) show that the domain structure of the sample consists of band domains after out-of-plane demagnetization (b), bubble domains in the $s = 0.3$ (c) and $s = 0.93$ (d) states. (From Lange *et al.* cond-mat/0310132).

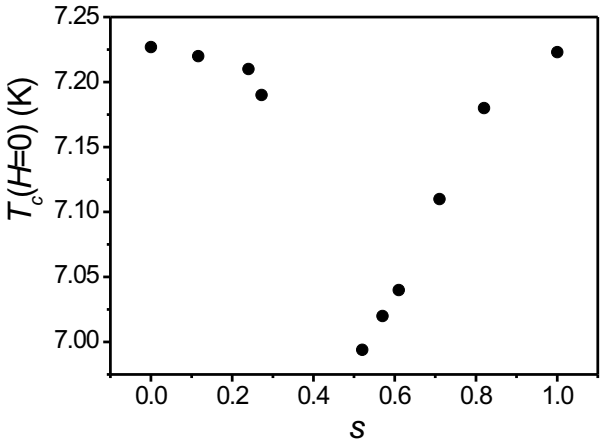

Figure 16: Dependence of the critical temperature at zero field T_c(H=0) on the parameter s. The minimum value of T_c is observed for $s = 0.5$. (From Lange *et al.* cond-mat/0310132)

through the percolating network. The strongly magnetized state, on the contrary, provides more regular vortex structure and enhances pinning.

3.3.5 Thick Films

Above we have discussed the case when both magnetic and superconducting films are thin, namely, $d_s \ll \lambda_L$ and $d_m \ll L_f$. In this subsection we briefly discuss, following works by Sonin [48], situation when both films are thick $d_s \gg \lambda_L$ and $d_m \gg L_f$. Below we neglect the domain wall width. Consider first the ferromagnetic film without superconductor. This problem has been solved exactly by Sonin [101]. Figure 17a shows schematically magnetic field distribution around thick ferromagnetic film. The problem can be solved by calculating field from "magnetic charges" on the magnetic film surface [48].

The magnetic field, without a superconducting substrate, at the ferromagnetic film boundary $y = 0^+$ is given by [48]:

$$H_x(x) = -4M \ln \left| \tan \frac{\pi x}{2L_f} \right| \ . \tag{80}$$

$$H_y(x) = \mp 2\pi M \text{sign} \left(\tan \frac{\pi x}{2L_f} \right) \text{at} \ \ y \to \pm 0 \ . \tag{81}$$

The field pattern is periodic with the period $2L_f$ along the axis x. The magnetic charge on the film boundary $y = 0$ is

$$\rho_M = -M\delta(y) \text{sign} \left(\tan \frac{\pi x}{2L_f} \right) \ . \tag{82}$$

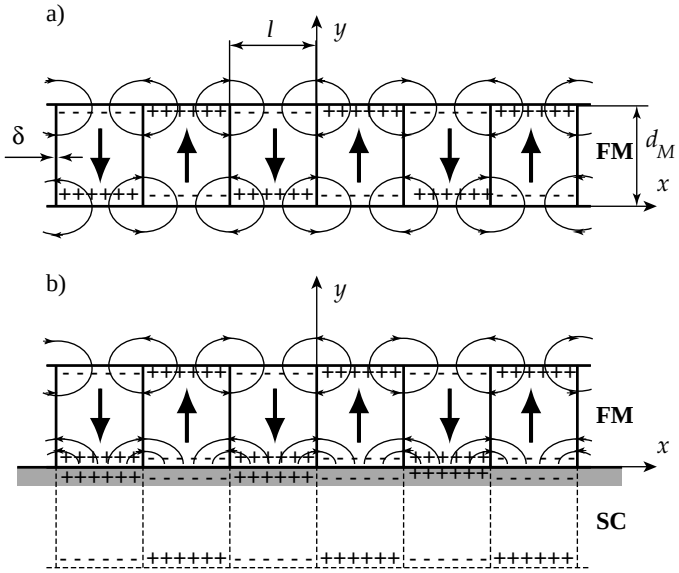

Figure 17: Magnetic charges (+ and -) and magnetic flux (thin lines with arrows) in a ferromagnetic film (FM) without (a) and with (b) a superconducting substrate (SC). The magnetization vectors in domains are shown by thick arrows. (From Sonin cond-mat/0102102)

Sonin has argued [48] that in the case of bulk superconductor and with additional requirement $\lambda_L/L_f \to 0$, the magnetic flux from the magnetic film is practically expelled from superconductor and problem can be solved by using images of magnetic charges on the magnetic film surface as shown in figure 17b. Sonin has calculated energy change due to presence of the superconducting substrate and concluded that the substrate increases the total magnetic energy by 1.5 times. The energy of the domain walls per unit length along the axis x is inversely proportional to domain width L_{fs} and the energy of the stray fields is proportional to L_{fs}. The domain width L_{fs} is determined by minimization of the total energy per unit length. The growth of the magnetic energy decreases the domain width L_{fs} by $\sqrt{1.5}$ times. Relative correction to the energy for finite λ_L/L_{fs} is of the order of λ_L/L_{fs} [48].

4 Proximity Effects in Layered Ferromagnet - Superconductor Systems

4.1 Oscillations of the order parameter

All oscillatory phenomena theoretically predicted and partly observed in the S/F layered systems are based on the Larkin-Ovchinnikov-Fulde-Ferrel (LOFF) effect first proposed for homogeneous systems with coexisting superconductivity and ferromagnetism [53, 54]. They predicted that the energy favorable superconducting order parameter in the presence of

exchange field should oscillate in space. The physical picture of this oscillation is as follows. In a singlet Cooper pair the electron with the spin projection parallel to the exchange field acquires the energy $-h$, whereas the electron with the antiparallel spin acquires the energy $+h$. Their Fermi momenta therefore split onto the value $q = 2h/v_F$. The Cooper pair acquires such a momentum and therefore its wave function is modulated. The direction of this modulation vector in the bulk superconductor is arbitrary, but in the S/F bilayer the preferential direction of the modulation is determined by the normal to the interface (z-axis). There exist two kinds of Cooper pairs differing with the direction of the momentum of the electron whose spin is parallel to the exchange field. The interference of the wave functions for these two kinds of pairs leads to the standing wave:

$$F(z) = F_0 \cos qz \tag{83}$$

A modification of this consideration for the case when the Cooper pair penetrates to a ferromagnet from a superconductor was proposed by Demler *et al.*[102]. They argued that the energy of the singlet pair is bigger than the energy of 2 electrons in the bulk ferromagnet by the value $2h$ (the difference of exchange energy between spin up and spin down electrons). It can be compensated if the electrons slightly change their momentum so that the pair will acquire the same total momentum $q = 2h/v_F$. The value $l_m = v_F/h$ called the magnetic length is a natural length scale for the LOFF oscillations in a clean ferromagnet. Anyway, equation (83) shows that the sign of the order parameter changes in the ferromagnet. This oscillation leads to a series of interesting phenomena that will be listed here and considered in some details in next subsections.

1. Periodic transitions from 0- to π phase in the S/F/S Josephson junction when varying thickness d_f of the ferromagnetic layer and temperature T.

2. Oscillations of the critical current vs. d_f and T.

3. Oscillations of the critical temperature vs. thickness of magnetic layer.

The penetration of the magnetized electrons into superconductors strongly suppresses the superconductivity. This obvious effect is accompanied with the appearance of magnetization in the superconductor. It penetrates on the depth of the coherence length and is directed opposite to magnetization of the F-layer. Another important effect which does not have oscillatory character and will be considered later is the preferential antiparallel orientation of the two F-layers in the S/F/S trilayer.

The described simple physical picture can be also treated in terms of the Andreev reflection at the boundaries[103], long known to form the in-gap bound states [93], [104]. Due to the exchange field the phases of Andreev reflection in the S/F/S junction are different than in junctions S/I/S or S/N/S (with non-magnetic normal metal N). Indeed, let consider a point P inside the F-layer at a distance z from one of the interfaces [105]. The pair of electrons emitted from this point at the angle $\pm\theta, \pm(\pi-\theta)$ to the z-axis will be reflected as a hole along the same lines and returns to the same point (figure 18). The interference of the Feynman amplitudes for these 4 trajectories creates an oscillating wave function of the Cooper pair.

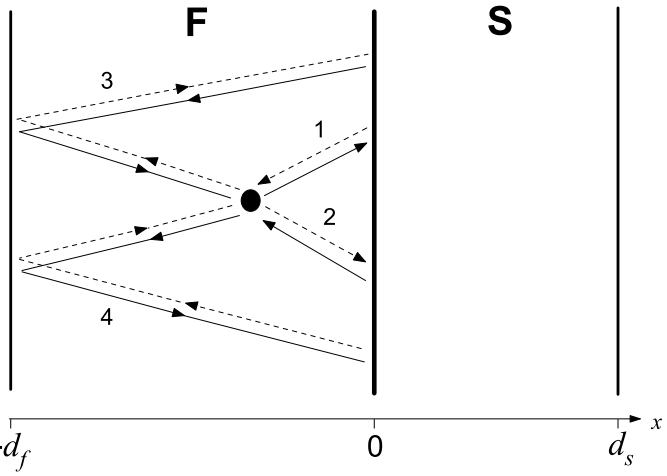

Figure 18: Four types of trajectories contributing (in the sense of Feynman's path integral) to the anomalous wave function of correlated quasiparticles in the ferromagnetic region. The solid lines correspond to electrons, the dashed lines — to holes; the arrows indicate the direction of the velocity. (From Fominov *et al.* cond-mat/0202280)

The main contribution to the total wave function arises from a small vicinity of $\theta = 0$. Taking only this direction, we find for the phases: $S_1 = -S_2 = -qz; S_3 = -S_4 = -q(2d_f - z)$. Summing up all Feynman's amplitudes $e^{iS_k}; k = 1...4$, we find the spatial dependence of the order parameter:

$$F \propto \cos qd_f \cos q(d_f - z) \tag{84}$$

At the interface $F \propto (\cos qd_f)^2$. It oscillates as a function of magnetic layer thickness with the period $\Delta d_f = \pi/q = 2\pi v_F/h$ and decays due to the interference of trajectories with different θ.

In a real experimental setup the LOFF oscillations are strongly suppressed by the elastic impurity scattering. The trajectories are diffusive random paths and simple geometrical picture is not more valid. However, as long as the exchange field h exceeds or is of the same order of magnitude as the scattering rate in the ferromagnet $1/\tau_f$, the oscillations do not disappear completely. Unfortunately, the experiments with strong magnets possessing large exchange fields are not reliable since the period of oscillations goes to the atomic scale. Two layers with different thickness when they are so thin can have different structural and electronic properties. In this situation it is very difficult to ascribe unambiguously the oscillations of properties to quantum interference.

4.2 Non-monotonic behavior of the transition temperature.

This effect was first predicted by Radovic *et al.* [63]. Its reason is the LOFF oscillations described in subsection 4.1. If the transparency of the S/F interface is low, one can expect

that the order parameter in the superconductor is not strongly influenced by the ferromagnet. On the other hand, the condensate wave function at the interface in the F-layer $F \propto (\cos 2d_f/\lambda_m)^2$ becomes zero at $d_f = \pi\lambda_m(n+1/2)/2$ (n is an integer). At this values of thickness the discontinuity of the order parameter at the boundary and together with it the current of Cooper pairs into the ferromagnet has a maximum. Therefore one can expect that the transition temperature is minimal [106]. Experimental attempts to observe this effect were made many times on the S/F multilayers Nb/Gd [107], Nb/Fe [108], V/V-Fe [109], V/Fe [110]. More references and details about these experiments and their theoretical description can be found in the cited reviews [60, 61]. Unfortunately, in these experiments the magnetic component was a strong ferromagnet and, therefore, they faced all the difficulties mentioned in subsection 3.3.1: the F-layer must be too thin and its variation produce uncontrollable changes in the sample, the influence of the growth defects is too strong. Besides, in multilayers the reason of the non-monotonous dependence of T_c on d_f may be the $0-\pi$ transition. Therefore, the reliable experiment should be performed with a bilayer possessing a sufficiently thick F-layer. Such experiments were performed recently [111, 112]. The idea was to use a weak ferromagnet (the dilute ferromagnetic alloy Cu-Ni) with rather small exchange field h to increase the magnetic length $l_m = \sqrt{D_f/h}$. They performed the experiments with S/F bilayers to be sure that the non-monotonic behavior is not originated from the $0-\pi$-transition. In these experiments the transparency of the interface was not too small or too large, the exchange field was of the same order as the temperature and the thickness of the F-layer was of the same order of magnitude as magnetic length. Therefore, for the quantitative description of the experiment theory should not be restricted by limiting cases only. Such a theory was developed by Fominov *et al.*[105]. In the pioneering work by Radovic *et al.* [63] the exchange field was assumed to be very strong.

As always when it goes about critical temperature, the energy gap and anomalous Green function F are infinitely small. Therefore one needs to solve linearized equations of superconductivity. The approach by Fominov *et al.* is based on solution of the linearized Usadel equation and is valid in the diffusion limit $\tau_s T_c \ll 1; \tau_f T_c \ll 1; \tau_f h \ll 1$. Namely this situation was realized in the cited experiments [111, 112]. The work by Fominov *et al.* [105] covers numerous works by their predecessors [66, 113, 114, 102, 106] clarifying and improving their methods. Therefore in the presentation of this subsection we follow presumably the cited work [105] and briefly describe specific results of other works.

The starting point is the linearized Usadel equations for singlet pairing for anomalous Green functions F_s in the superconductor and F_f in the ferromagnet:

$$D_s \frac{\partial^2 F_s}{\partial z^2} - |\omega_n| F_s + \Delta = 0; 0 < z < d_s. \tag{85}$$

$$D_f \frac{\partial^2 F_f}{\partial z^2} - (|\omega_n| + ih\mathrm{sgn}\omega_n) F_f = 0; -d_f < z < 0. \tag{86}$$

Thus, we accept a simplified model in which $\Delta = 0$ in the ferromagnetic layer and $h = 0$ in the superconducting one. The geometry is schematically shown in figure 19.

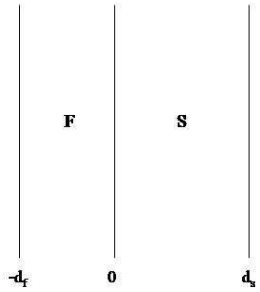

Figure 19: FS bilayer. The F and S layers occupy the regions $-d_f < z < 0$ and $0 < z < d_s$, respectively.

Equations (86,85) must be complemented with the self-consistency equation:

$$\Delta(\mathbf{r}) \ln \frac{T_{cs}}{T} = \pi T \sum_n \left(\frac{\Delta(\mathbf{r})}{|\omega_n|} - F_s(\omega_n, \mathbf{r}) \right), \tag{87}$$

where T_{cs} is the bulk SC transition temperature, and with linearized boundary conditions at the interface:

$$\sigma_s \frac{dF_s}{dz} = \sigma_f \frac{dF_f}{dz} \tag{88}$$

$$\mathcal{A}\sigma_f \frac{dF_f}{dz} = G_b \left(F_s(0) - F_f(0) \right), \tag{89}$$

where $\sigma_{s,f}$ is the conductivity of the superconducting (ferromagnetic) layer in the normal state; G_b is the conductance of the interface and $\mathcal{A}$ is the area of the interface. We assume that the normal derivative of the anomalous Green function is equal to zero at the interface with the vacuum:

$$\frac{dF_f}{dz}|_{z=-d_f} = \frac{dF_s}{dz}|_{z=d_s} = 0 \tag{90}$$

The condition of solvability of linear equations (85,86,87) with the boundary conditions (88,89,90) determines the value of transition temperature T_c for the F/S bilayer.

The solution $F_f(\omega_n, z)$ in the F-layer satisfying the boundary condition (90) reads:

$$F_f(\omega_n, z) = C(\omega_n) \cosh[k_{fn}(z + d_f)]; \;\; k_{fn} = \sqrt{\frac{|\omega_n| + ih\mathrm{sgn}\omega_n}{D_f}}, \tag{91}$$

where $C(\omega_n)$ is the integration constant to be determined from the matching condition at the F/S interface $z = 0$. From the two boundary conditions at $z = 0$ (88,89) it is possible to eliminate F_f and dF_f/dz and reduce the problem to finding the function F_s from equation (85) and the effective boundary condition at $z = 0$:

$$\xi_s \frac{dF_s}{dz} = \frac{\gamma}{\gamma_b + B_f(\omega_n)} F_s; \tag{92}$$

where $\xi_s = \sqrt{D_s/(2\pi T_{cs}}; \gamma = \sigma_f/\sigma_s; \gamma_b = (\mathcal{A}\sigma_f)/(\xi_s G_b)$ and $B_f(\omega_n) = (k_{fn}\xi_s \tanh(k_{fn}d_f))^{-1}$. Since k_{fn} is complex the parameter $B_f(\omega_n)$ and consequently the function F_s is complex. The coefficients of the Usadel equation (85) are real. Therefore, it is possible to solve it for the real part of the function F_s traditionally denoted as $F_s^+(\omega_n, z) \equiv \frac{1}{2}\left(F_s(\omega_n, z) + F_s(-\omega_n, z)\right)$. The boundary condition for this function reads:

$$\xi_s \frac{dF_s^+}{dz} = W(\omega_n) F_s^+|_{z=0}; \;\; W(\omega_n) = \frac{A_{sn}(\gamma_b + \Re B_f) + \gamma}{A_{sn}|\gamma_b + B_f|^2 + \gamma(\gamma_b + \Re B_f)}, \tag{93}$$

where $A_{sn} = k_{sn}d_s \tanh(k_{sn}d_s)$ and $k_{sn} = \sqrt{\frac{D_s}{|\omega_n|}}$. To derive this boundary condition we accept the function $\Delta(z)$ to be real (it will be justified later). Then the imaginary part of the anomalous Green function $F_s^-(\omega_n, z)$ obeys the homogeneous linear differential equation;

$$\frac{d^2F_s^-}{dz^2} = k_{sn}^2 F_s^-$$

and the boundary condition $\frac{dF_s^-}{dz} = 0$ at $z = d_s$. Its solution is $F_s^-(\omega_n, z) = E(\omega_n)\cosh[k_{sn}(z - d_s)]$. At the interface $z = 0$ its derivative $\frac{dF_s^-}{dz}|_{z=0}$ is equal to $-k_{sn}\tanh(k_{sn}d_s)F_s^-(\omega_n, z = 0)$. Eliminating F_s^- and its derivative from real and imaginary parts of the boundary condition (92), we arrive at the boundary condition (93). Note that only F_s^+ participates in the self-consistence equation (87). This fact serves as justification of our assumption on reality of the order parameter $\Delta(z)$.

Simple analytic solutions of the problem are available for different limiting cases. Though these cases are unrealistic at the current state of experimental art, they help to understand the properties of the solutions and how do they change when parameters vary. Let us consider the case of very thin S-layer $d_s \ll \xi_s$. In this case the order parameter Δ is almost a constant. The solution of equation (85) in such a situation is $F_s^+(\omega_n, z) = -\frac{\Delta}{|\omega_n|} + \alpha_n \cosh k_{sn}(z - d_s)$, where α_n is an integration constant. From the boundary condition (93) we find:

$$\alpha_n = -\frac{2\Delta W(\omega_n)}{|\omega_n|\left(A_{sn} + W(\omega_n)\right)}, \tag{94}$$

where the coefficients A_{sn} are the same as in equation (93). We assume that $k_{sn}d_s \ll 1$. Then $A_{sn} \approx k_{sn}^2 \xi_s d_s = \frac{d_s}{\xi_s}(n + 1/2)$. The function $F_s^+(\omega_n, z)$ almost does not depend on z. The self-consistence equation reads:

$$\ln\frac{T_{cs}}{T_c} = 2\sum_{n\geq 0} \frac{W(\omega_n)}{(n + \frac{1}{2})\left(\frac{d_s}{\xi_s}(n + \frac{1}{2}) + W(\omega_n)\right)} \tag{95}$$

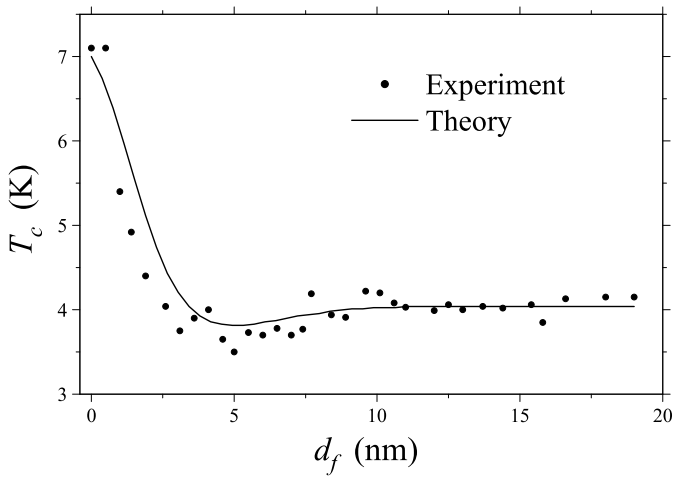

Figure 20: Theoretical fit to the experimental data. (From Fominov *et al.* cond-mat/0202280).

The summation can be performed explicitly in terms of digamma-functions (F):

$$\ln\frac{T_{cs}}{T_c}=\frac{\gamma\xi_s}{2(\gamma_b+\Re B_f)d_s}\Re\left\{\left(1-\frac{i(\gamma_b+\Re B_f)}{\Im B_f}\right)\left[\mathsf{F}\left(\frac{1}{2}+\frac{\gamma\xi_s}{d_s}\left(1-\frac{i\Im B_f}{\gamma_b+\Re B_f}\right)\right)-\mathsf{F}(\frac{1}{2})\right]\right\}. \tag{96}$$

Possible oscillations are associated with the coefficients B_f. If the magnetic length $\lambda_m=\sqrt{D_f/h}$ is much less than d_f, then $B_f\approx\sqrt{\frac{h}{4\pi T_{cs}}}\exp(-\frac{2id_f}{\lambda_m}-\frac{i\pi}{4})$. In the opposite limiting case $\lambda_m\gg d_f$ there are no oscillations of the transition temperature. Note that $\ln(T_{cs}/T_c)$ can be rather large $\sim\xi_s/d_s$, i.e the transition temperature in the F/S bilayer with very thin S-layer can be exponentially suppressed. This tendency is reduced if the resistance of the interface is large ($\gamma_b\gg 1$).

In a more realistic situation considered in the work [105] neither of parameters $d_s/\xi_s, d_f/\lambda_m, \gamma, \gamma_b$ is very small or very large and an exact method of solution should be elaborated. The authors propose to separate explicitly the oscillating part of the functions $F_s^+(\omega_n,z)$ and $\Delta(z)$ and the reminders:

$$F_s^+(\omega_n,z)=f_n\frac{\cos q(z-d_s)}{\cos qd_s}+\sum_{m=1}^{\infty}f_{nm}\frac{\cosh q_m(z-d_s)}{\cosh q_md_s} \tag{97}$$

$$\Delta(z)=\delta\frac{\cos q(z-d_s)}{\cos qd_s}+\sum_{m=1}^{\infty}\delta_m\frac{\cosh q_m(z-d_s)}{\cosh q_md_s} \tag{98}$$

where the wave-vectors q and q_m as well as the coefficients of the expansion must be found from the boundary conditions and self-consistence equation. Equation (93) results in relations between coefficients of the expansion:

$$f_n=\frac{\delta}{|\omega_n|+D_sq^2};\quad f_{nm}=\frac{\delta_m}{|\omega_n|-D_sq_m^2}. \tag{99}$$

Substituting the values of coefficients f_n, f_{nm} from equation (99) to the boundary condition (93), we find an infinite system of homogeneous linear equations for coefficients δ and δ_m:

$$\delta \frac{q \tan q d_s - W(\omega_n)}{|\omega_n| + D_s q^2} + \sum_{m=1}^{\infty} \delta_m \frac{q_m \tanh q_m d_s - W(\omega_n)}{|\omega_n| - D_s q_m^2} \tag{100}$$

Equating the determinant of this system $\mathcal{D}$ to zero, we find a relation between q and q_m. It is worthwhile to mention a popular approximation adopted by several theorists [66, 102, 106] the so-called single-mode approximation. In our terms it means that all coefficients $\delta_m, m = 1, 2...$ are zero and only the coefficient δ survives. The system (100) implies that it is only possible when the coefficients $W(\omega_n)$ do not depend on their argument ω_n. It happens indeed in the limit $d_s/\xi_s \ll 1$ and $h \gg T$. For a more realistic regime the equation $\mathcal{D} = 0$ must be solved numerically together with the self-consistence condition, which turns into a system of equations:

$$\begin{aligned} \ln \frac{T_{cs}}{T_c} &= \mathsf{F}\left(\frac{1}{2} + \frac{D_s q^2}{T_c}\right) - \mathsf{F}(\frac{1}{2}) \\ \ln \frac{T_{cs}}{T_c} &= \mathsf{F}\left(\frac{1}{2} - \frac{D_s q_m^2}{T_c}\right) - \mathsf{F}(\frac{1}{2}) \end{aligned} \tag{101}$$

These systems were truncated and solved with all data extracted from the experimental setup used by Ryazanov *et al.* [112]. The only 2 fitting parameters were $h = 130K$ and $\gamma_b = 0.3$.

Figure 20 demonstrates rather good agreement between theory and experiment. Various types of the curves $T_c(d_f)$ are shown in figure 21. Note that the minimum on these curves eventually turns into a plateau at $T_c = 0$, the reentrant phase transition into the superconducting state. Some of the curves have a well-pronounced discontinuity, which can be treated as the first order phase transition. The possibility of the first order transition to superconducting state in the F/S bilayer was first indicated by Radovic *et al.* [63].

4.3 Josephson effect in S/F/S junctions

As we already mentioned the exchange field produces oscillations of the order parameter inside the F-layer. This effect in turn can change the sign of the Josephson current in the S/F/S junction compared to the standard S/I/S or S/N/S junctions. As a result the relative phase of the S-layers in the ground state is equal to π (the so-called π-junction). In the closed superconducting loop with such a junction spontaneous magnetic flux and spontaneous current appear in the ground state. These phenomena were first predicted by Bulaevsky *et al.* [55] for π-junction independently on the way of its realization. Buzdin *et al.* [56] have first argued that such a situation can be realized in the S/F/S junction at a proper choice of its length. Ryazanov *et al.* [57, 58] have realized such a situation employing the weak ferromagnet Cu_xNi_{1-x} as a ferromagnetic layer. A similar approach was used by Kontos *et al.* [59], who used a diluted alloy PdNi. The weakness of exchange field allowed them to drive the oscillations and in particular the 0-π transition by the temperature at a

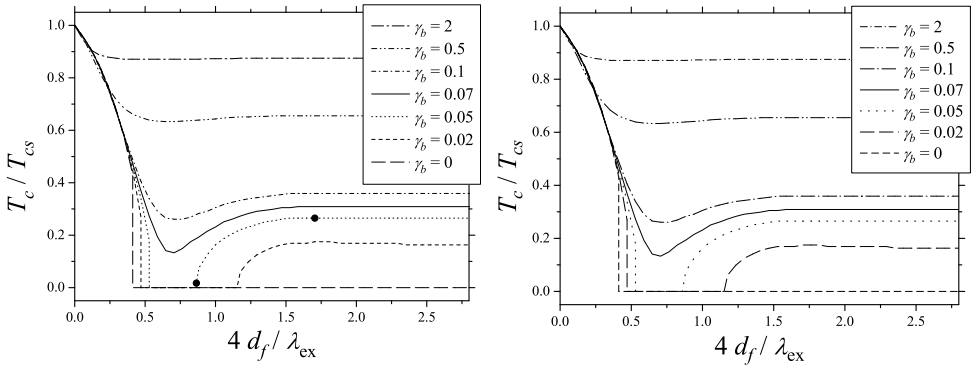

Figure 21: Theoretical fit to the experimental data. (From Fominov *et al.* cond-mat/0202280).

fixed magnetic field. The success of this experiment have generated an extended literature. The theoretical and experimental study of this and related phenomena still are active. In what follows we present a brief description of relevant theoretical ideas and the experiments.

4.3.1 Simplified approach and experiment

Here we present a simplified picture of the S/F/S junction based on the following assumptions:
i)The transparency of the S/F interfaces is small. Therefore the anomalous Green function in the F-layer is small and it is possible to use the linearized Usadel equation.
ii) The energy gap Δ inside each of the S- layers is constant and equal to $\Delta_0 e^{\mp i\varphi/2}$ (the sign $-$ relates to the left S-layer, $+$ to the right one).
iii) $\Delta = 0$ in the F-layer and $h = 0$ in the S-layers.
The geometry of the system is shown in figure (19). From the second assumption it follows that the anomalous Green function F is also constant within each of S-layers: $F = \frac{\Delta}{\sqrt{|\omega_n|^2+\Delta_0^2}}$.
The linearized Usadel equation in the F-layer (86) has a following general solution:

$$F(\omega_n, z) = \alpha_n e^{k_{fn} z} + \beta_n e^{-k_{fn} z}, \tag{102}$$

where

$$k_{fn} = \sqrt{\frac{|\omega_n| + ih\mathrm{sgn}\omega_n}{D_f}} \tag{103}$$

(compare equation (91)). The boundary condition at the two interfaces follows from the second boundary condition of the previous section (89) in which F_f is neglected:

$$\xi_f \frac{dF_f}{dz} = \mp \gamma_b F_s \tag{104}$$

The coefficients α_n and β_n are completely determined by the boundary conditions (104):

$$\alpha_n = Q_n \frac{\cos(\frac{\varphi - ik_{fn}d_f}{2})}{sinh(k_{fn}d_f)} \tag{105}$$

$$\beta_n = Q_n \frac{\cos(\frac{\varphi + ik_{fn}d_f}{2})}{sinh(k_{fn}d_f)} \tag{106}$$

where $Q_n = \frac{\Delta_0}{\gamma_b \xi_f k_{fn} \sqrt{|\omega_n|^2 + \Delta_0^2}}$. Equation (34) for the electric current must be slightly modified to incorporate the exchange field h:

$$\mathbf{j} = ie\pi T N(0) D \sum_n (\tilde{F}\hat{\partial}F - F\hat{\partial}\tilde{F}), \tag{107}$$

where $\tilde{F}(\omega_n, z) = F^*(-\omega_n, z)$. Note that at this transformation the wave vectors k_{fn} remain invariant. After substitution of the solution (102) we find that $j = j_c \sin\varphi$ with the following expression for the critical current [114, 115, 57]:

$$j_c = \frac{4\pi T \Delta_0^2}{eR_N \Gamma_b} \Re \left[\sum_{\omega_n > 0} \left((\omega_n^2 + \Delta_0^2) k_{fn} d_f sinh(k_{fn} d_f) \right)^{-1} \right], \tag{108}$$

where R_N is the normal resistance of the ferromagnetic layer and Γ_b is the dimensionless parameter characterizing the ratio of the interface resistance to that of the F-layer. Kupriyanov and Lukichev [85] have found the relationship between Γ_b and the the barrier transmission coefficient $D_b(\theta)$ (θ is the angle between the electron velocity and the normal to the interface):

$$\Gamma_b = \frac{2l_f}{3d_f} \langle \frac{\cos\theta D_b(\theta)}{1 - D_b(\theta)} \rangle. \tag{109}$$

As we explained earlier, the oscillations appear since k_{fn} are complex values. If $h \gg 2\pi T$ ω_n, then $k_{fn} \approx (1+i)\sqrt{\frac{h}{2D_f}}$ and oscillations are driven only by the thickness. It was very important to use a weak ferromagnet with exchange field h comparable to πT. Then the temperature also drives the oscillations. In the Cu-Ni alloys used in the experiment [57] the Curie point T_m was between 20 and 50K. Nevertheless, the ratio $h/\pi T$ was in the range of 10 even for the lowest T_m. In this situation k_{fn} does not depend on n for the large number of terms in the sum (108). This is the reason why the sum in total is periodic function of d_f with the period $\lambda_m = \pi\sqrt{2D_f/h}$. The dependence on temperature is generally weak. However, if the thickness is close to the value at which j_c turns into zero at $T = 0$, the variation of temperature can change the sign of j_c.

In figure (22b) theoretical curves $j_c(T)$ from cited work [105] are compared with the experimental data by Ryazanov *et al.* [57, 76]. The curves are plots of the modulus of j_c vs T. Therefore, the change of sign of j_c is seen as a cusp on such a curve. At temperature of the cusp the transition from 0- to π-state of the junction proceeds. The change of sign is clearly seen on the curve corresponding to $d_f = 27nm$. The experimental S/F/S junction

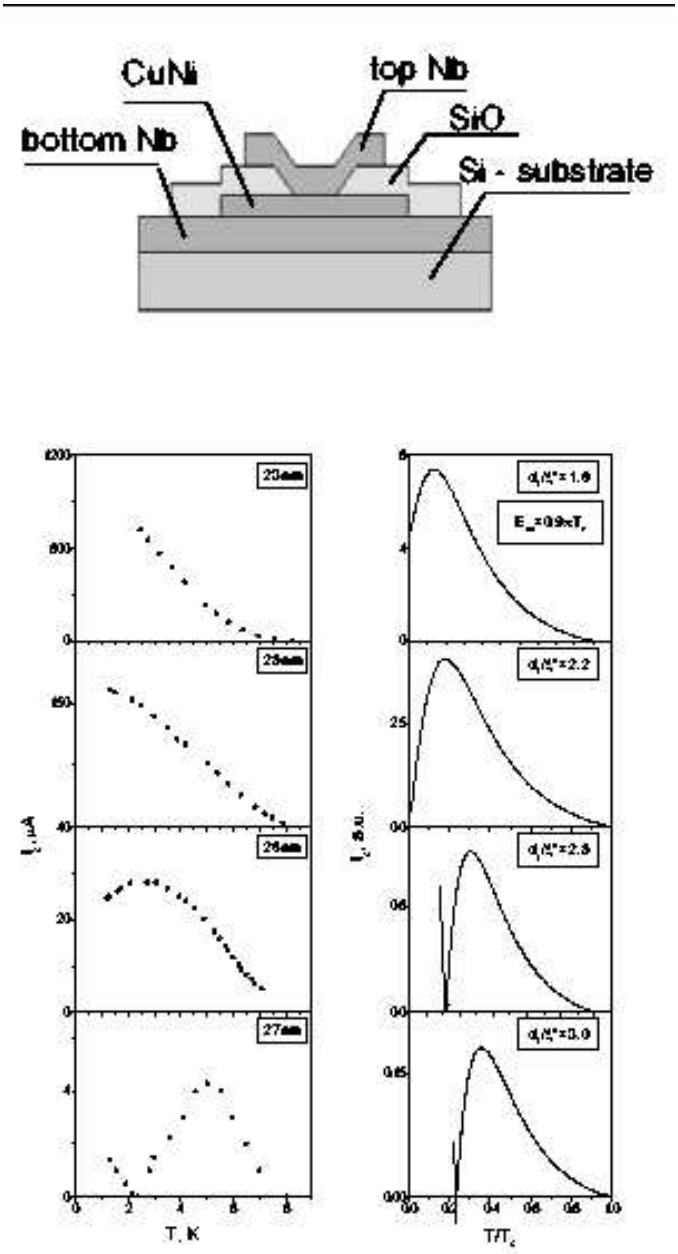

Figure 22: (Upper) Schematic cross-section of the sample. (Lower) Left : critical current Ic as function of temperature for $Cu_{0.48}Ni_{0.52}$ junctions with differ- ent F-layer thicknesses between 23 nm and 27 nm as indicated. Right : model calculations of the tem- perature dependence of the critical current in an SFS junction. (From Ryazanov *et al.* cond-mat/0008364)

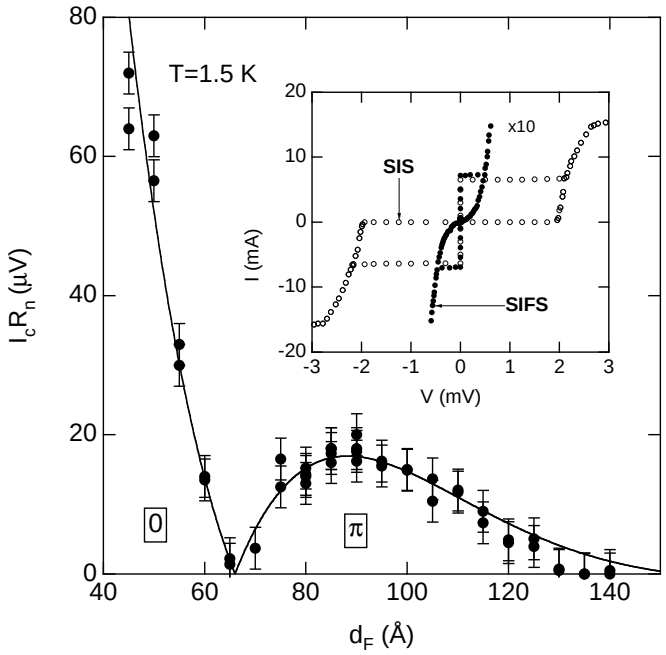

Figure 23: Josephson coupling as a function of thickness of the PdNi layer (full circles). The critical current cancels out at $d_F \simeq 65$ Å indicating the transition from "0" to "π"-coupling. The full line is the best fit obtained from the theory as described in the text. Insert shows typical I-V characteristics of two junctions with (full circles), and without (empty circles) PdNi layer. (From Kontos *et al.* cond-mat/0201104).

is schematically shown in figure (22a). The details of the experiment are described in original paper [57] and in reviews [76, 60]. Not less impressive agreement between theory and experiment is reached by Kontos *et al.* [59] (theory was given by T. Kontos) (see figure 23).

Very good agreement with the same experiment was reached in a recent theoretical work by Buzdin and Baladie [116] who solved the Eilenberger equation.
Zyuzin *et al.* [117] have found that in a dirty sample the amplitude of the Josephson current j_c is a random value with an indefinite sign. They estimated the average square fluctuations of this amplitude for the interval of the F-layer thickness $\xi_s < d_f < \sqrt{D/T}$ as:

$$\langle j_c^2 \rangle = \mathcal{A}\xi_s^2 \left(\frac{g}{8\pi N(0) D_f} \right)^4 \left(\frac{D_f}{2\pi^2 T d_f^2} \right)^2 \tag{110}$$

where $\mathcal{A}$ is the area of interface and g is its conductance per unit area. The fluctuations are significant when d_f becomes smaller than the diffusive thermal length $\sqrt{D/T}$.

4.3.2 Josephson effect in a clean system

In a recent work by Radovic *et al* [118] considered the same effect in a clean S/F/S trilayer. A similar, but somewhat different in details approach was developed by Halterman and Olives [119]. The motivation for this consideration is the simplicity of the model and very clear representation of the solution. Though in the existing experimental systems the oscillations are not disguised by impurity scattering, it is useful to have an idea what maximal effect could be reached and what role plays the finite transparency of the interface. The authors employed the simplest version of theory, Bogolyubov-DeGennes equations:

$$\hat{H} \begin{pmatrix} u_\sigma \\ v_{\bar{\sigma}} \end{pmatrix} = E \begin{pmatrix} u_\sigma \\ v_{\bar{\sigma}} \end{pmatrix}, \tag{111}$$

where $\bar{\sigma}$ means $-\sigma$ and the effective Hamiltonian reads:

$$\hat{H} = \begin{pmatrix} H_0(\mathbf{r}) - \sigma h(\mathbf{r}) & \Delta(\mathbf{r}) \\ \Delta^*(\mathbf{r}) & -H_0 + \sigma h(\mathbf{r}) \end{pmatrix}, \tag{112}$$

$$H_0(\mathbf{r}) = -\frac{\hbar^2}{2m}\nabla^2 - \mu + W(\mathbf{r}) \tag{113}$$

In the last equation μ is the chemical potential and $W(\mathbf{r})$ is the barrier potential:

$$W(\mathbf{r}) = W[\delta(z + d/2) + \delta(z - d/2)]. \tag{114}$$

The assumption about exchange field $h(\mathbf{r})$ and the order parameter $\Delta(\mathbf{r})$ are the same as in the previous subsubsection. We additionally assume that the left and right S-layers are identical and semi-infinite extending from $z = -\infty$ to $z = -d/2$ and from $z = d/2$ to $z = \infty$. Due to translational invariance in the (x, y)-plane the dependence of the solution on the lateral coordinates is a plane wave:

$$\begin{pmatrix} u_\sigma \\ v_\sigma \end{pmatrix} = e^{i\mathbf{k}_\parallel \mathbf{r}} \Psi(z) \tag{115}$$

There are 8 fundamental solutions of these equations corresponding to the injection of the quasiparticle or quasihole from the left or from the right with spin up or down. We will write explicitly one of them $\Psi_1(z)$, corresponding to the injection of the quasiparticle from the right. In the superconducting area $z < -d/2$ we will see the incident quasiparticle wave with the coefficient 1 and the normal wave vector k^+, the reflected quasiparticle with the reflection coefficient b^+ and the normal wave vector $-k^+$; the reflected quasihole (Andreev reflection) with the reflection coefficient a_1 and the wave vector k_-, where $(k^\pm)^2 = \frac{2m}{\hbar^2}(E_F \pm \xi)^2 - \mathbf{k}_\parallel^2$, E_F is the Fermi energy and $\xi = \sqrt{E^2 - |\Delta|^2}$. Thus the solution $\Psi_1(z)$ at $z < -d/2$ reads:

$$\Psi_1(z) = (e^{ik^+z} + b_1 e^{-ik^+z}) \begin{pmatrix} ue^{-i\varphi/2} \\ ve^{i\varphi/2} \end{pmatrix} + a_1 e^{ik^-z}) \begin{pmatrix} ve^{-i\varphi/2} \\ ue^{i\varphi/2} \end{pmatrix} \tag{116}$$

where u and v are the bulk Bogolyubov-Valatin coefficients: $u = \sqrt{(1+\xi/E)/2}; v = \sqrt{(1-\xi/E)/2}$. In the F-layer $-d/2 < z < d/2$ there appear transmitted and reflected electron and transmitted and reflected hole. Since according to our assumption $\Delta = 0$ in the F-layer, there is no mixing of the electron and hole. With this explanation we can write directly the solution $\Psi_1(z)$ in the F-layer:

$$\Psi_1(z) = (C_1 e^{iq^+z} + C_2 e^{iq^+z}) \begin{pmatrix} 1 \\ 0 \end{pmatrix} + (C_3 e^{iq_\sigma^- z} + C_4 e^{iq_\sigma^- z}) \begin{pmatrix} 0 \\ 1 \end{pmatrix}, \tag{117}$$

where $q_\sigma^\pm = \sqrt{\frac{2m}{\hbar^2}(E_F^f + \sigma h \pm E) - \mathbf{k}_\parallel^2}$. Finally in the right S-layer $z > d/2$ only the transmitted quasiparticle and quasihole propagate:

$$\Psi_1(z) = c_1 e^{ik^+z} \begin{pmatrix} ue^{i\varphi/2} \\ ve^{-i\varphi/2} \end{pmatrix} + d_1 e^{-ik^-z} \begin{pmatrix} ve^{i\varphi/2} \\ ue^{-i\varphi/2} \end{pmatrix} \tag{118}$$

The value of all coefficients can be established by matching of solutions at the interfaces:

$$\Psi(\pm\frac{d}{2} - 0) = \Psi(\pm\frac{d}{2} + 0); \;\; \frac{d\Psi}{dz}|_{\pm\frac{d}{2}+0} - \frac{d\Psi}{dz}|_{\pm\frac{d}{2}-0} = \frac{2mW}{\hbar^1}\Psi \tag{119}$$

Other fundamental solutions can be found by symmetry relations:

$$a_2(\varphi) = a_1(-\varphi); a_3 = a_2; a_4 = a_1; b_3 = b_1; b_4 = b_2, \tag{120}$$

where index 2 relates to the hole incident from the left, indices 3,4 relate to the electron and hole incident from the right. Each mode generates the current independently on others. The critical current reads:

$$j_c = i\frac{e\Delta T}{\hbar} \sum_{\sigma,\omega_n,\mathbf{k}_\parallel} \frac{k_n^+ + k_n^-}{2\xi_n} \left(\frac{a_{1n}}{k_n^+} - \frac{a_{2n}}{k_n^-} \right). \tag{121}$$

Here all the values with the index n mean functions of energy E denoted by the same symbols in which E is substituted by $i\omega_n$, for example $\xi_n = i\sqrt{\omega_n^2 + \Delta^2}$. We will not demonstrate

here straightforward, but somewhat cumbersome calculations and transit to conclusions. The critical current displays oscillations originated from two different types of the bound states. One of them appears if the barrier transmission coefficient is small. This is the geometrical resonance. The superconductivity is irrelevant for it. Another one appears even in the case of ideal transmission: this is the resonance due to the Andreev reflection. When the transmission coefficient is not small and not close to 1, it is not easy to separate these two type of resonances and the oscillations picture becomes rather chaotic. The LOFF oscillations are better seen when transmission coefficient is close to 1 since geometrical resonances do not interfere. Varying the thickness, one observes periodic transitions from 0 to π-state with the period equal to $\lambda_f/2 = 2\pi v_F/h$. The lowest value of d at which $0-\pi$-transition takes place is approximately $\lambda_f/4$. The temperature changes this picture only slightly, but near the thickness corresponding the $0-\pi$-transition the non-monotonic behavior of j_c vs. temperature including temperature driven $0-\pi$-transition can be found.
An intermediate case between the diffusion and clean limits was considered by Bergeret *et al.* [120]. They assumed that the F-layer is so clean that $h\tau_f \gg 1$, whereas $T_c\tau_s \ll 1$. Therefore Usadel equation is not valid for the F-layer and they solved the Eilenberger equation. They have found that the superconducting condensate oscillates as function of the thickness with period λ_f and penetrates into the F-layer over the depth equal to the electron mean free path l_f. The period of oscillations of the critical current is $\lambda_f/2$. No qualitative differences with considered cases appear unless the magnetization is inhomogeneous. Even very small inhomogeneity can completely suppress the $0-\pi$-transitions. This is a consequence of the generation of the triplet pairing, which will be considered later.

4.3.3 Half-integer Shapiro steps at the $0-\pi$ transition

Recently Sellier *et al.* [121] have reported the observation of the Shapiro steps at the voltage equal to half-integer of the standard values $V_n = n\hbar\omega/2e$, where ω is the frequency of the applied ac current. Let us remind that the standard (integer) Shapiro steps appear as a consequence of the resonance between the external ac field and the time-dependent Josephson energy $E_J = -\frac{\hbar j_c}{ed_f} cos\varphi(t)$ where the phase is proportional to time due to external permanent voltage through the contact: $\varphi(t) = 2eVt/\hbar$. Just in the $0-\pi$ transition point j_c turns into zero. Then the next term in the Fourier-expansion of the Josephson energy proportional to $\cos(2\varphi)$ dominates. That means that the Josephson current is proportional to $\sin(2\varphi)$. Such a term leads to the Shapiro steps not only at integer, but also at half-integer values since the resonance now happens at $(4eV/\hbar) = \omega$. Normally the term with $\sin(2\varphi)$ is so small that it was always assumed to vanish completely. The resonance hf method used by the authors had sufficient sensitivity to discover this term.
The authors prepared the $Nb/Cu_{52}Ni_{48}/Nb$ junction by the photolitography method. Curie temperature of the F-layer is 20K. The 2 samples they used had the thicknesses 17 and 19 nm. The $0-\pi$ transition was driven by temperature. The transition temperature in the first and second sample were 1.12 and 5.36K, respectively. The external ac current had the frequency $\omega = 800$ kHz and amplitude about 18 μA. The voltage current curves for $d_f = 17nm$ and temperatures close to 1.12 K are shown in figure (24). The fact that the

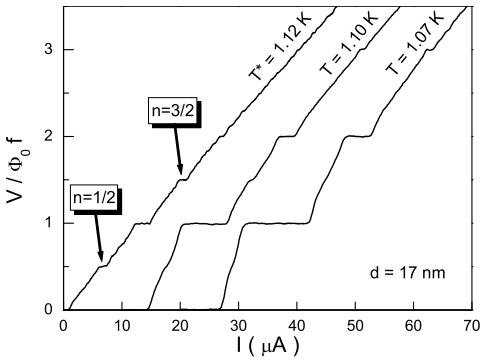

Figure 24: Shapiro steps in the voltage-current curve of a 17 nm thick junction with an excitation at 800 kHz (amplitude about 18 μA). Half-integer steps (n=1/2 and n=3/2) appear at the $0-\pi$ crossover temperature T^*. Curves at 1.10 and 1.07 K are shifted by 10 and 20 μA for clarity. (From Sellier *et al.* cond-mat/0406236).

half-integer steps disappear at very small deviation from the transition temperature proves convincingly that it is associated with the $0-\pi$ transition.

4.3.4 Spontaneous current and flux in a closed loop

Bulaevsky *et al.* [55] argued that a closed loop containing the π-junction may carry a spontaneous current and flux in the ground state. Below we reproduce their arguments. The energy of the closed superconducting loop depends on the total flux Φ through the loop:

$$E(\Phi) = -\frac{\hbar}{2e} J_c \cos\varphi + \frac{\Phi_0^2 \varphi^2}{8\pi^2 L c^2}, \tag{122}$$

where $\varphi = \frac{2\pi\Phi}{\Phi_0}$, J_c is the critical current and L is the inductance of the loop. The first term in equation (122) is the Josephson energy, the second is the energy of magnetic field. The location of the energy minimum depends on the the parameter $k = \frac{\Phi_0}{4\pi L J_c c}$. If k is positive, there is only one minimum at $\varphi = 0$. If $k < -1$, the only minimum is located again at $\varphi = 0$. If $-1 < k < 0$, the minimum is located at the nonzero root of equation $\sin\varphi/\varphi = |k|$; the value $\varphi = 0$ corresponds to a maximum of energy. Thus, the spontaneous flux appears at sufficiently large inductance of the loop. It is possible to avoid this limitation measuring the dependence of the current inside the loop on the external flux through it [58].

They used triangular bridge array with π-junctions in each shoulder (see Figs. 25). Due to the central π-junction the phases of the current in two sub-loops of the bridge differ by π. Therefore the critical current between the two contacts of the bridge is equal to zero in the absence of magnetic field. If the flux inside the loop reaches half of flux quantum, it compensates the indicated phase difference and the currents from both sub-loops are in the same phase. Thus, the shift of the current maximum from $\Phi = 0$ to $\Phi = \Phi_0/2$ is the direct evidence of the $0-\pi$ transition. Such experimental evidence was first obtained in the same work [57].

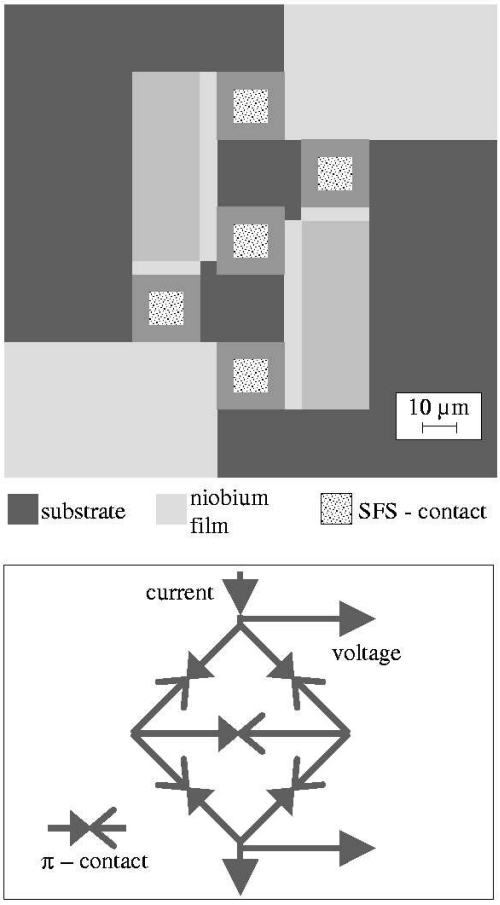

Figure 25: Real (upper) and schematic (low) picture of the network of five SFS junctions $Nb - Cu_{0.46}Ni_{0.54} - Nb$ ($d_F = 19$ nm), which was used in the phase-sensitive experiment. (From From Ryazanov *et al.* cond-mat/0103240).

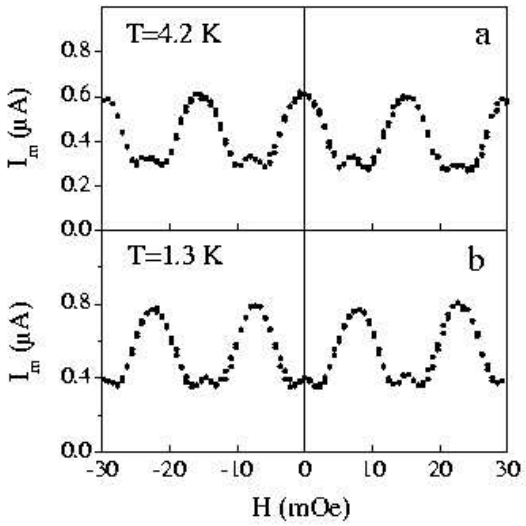

Figure 26: Magnetic field dependences of the critical transport current for the structure depicted in figure 25 at temperature above (a) and below (b) T_{cr}. (From From Ryazanov *et al.* cond-mat/0103240).

The graphs of the current vs magnetic field for two different temperatures (figure 26) clearly demonstrates the shift of the current maximum from zero to non-zero magnetic field. The next graph figure 27 shows the shift of the flux through the loop 0 to 1/2 of the flux quantum at the temperature driven $0 - \pi$ transition.

4.4 F/S/F junctions

The trilayers F/N/F (N is normal non-magnetic metal) have attracted much attention starting from the discovery by Grünberg [122] of the Giant Magnetoresistance (GMR). The direction of magnetization of ferromagnetic layers in these systems may be either parallel or antiparallel in the ground state oscillating with the thickness of the normal layer on the scale of few nanometers. The mutual orientation can be changed from antiparallel to parallel by a rather weak magnetic field. Simultaneously the resistance changes by the relative value reaching 50%. This phenomenon has already obtained a technological application in the magnetic transistors and valves used in computers [123]. A natural question is what happens if the central layer is superconducting: will it produce the spin-valve effect (a preferential mutual orientation of F-layers magnetization) and how does it depend on thicknesses of S and F-layers? This question was considered theoretically by several authors [64, 65, 66, 86, 124]. Recently the spin-valve effect was experimentally observed by Tagirov *et al.* [125].
Even without calculations it is clear that, independently on the thicknesses of S and F layers, the antiparallel orientation of magnetizations in F-layers has always lower energy than the

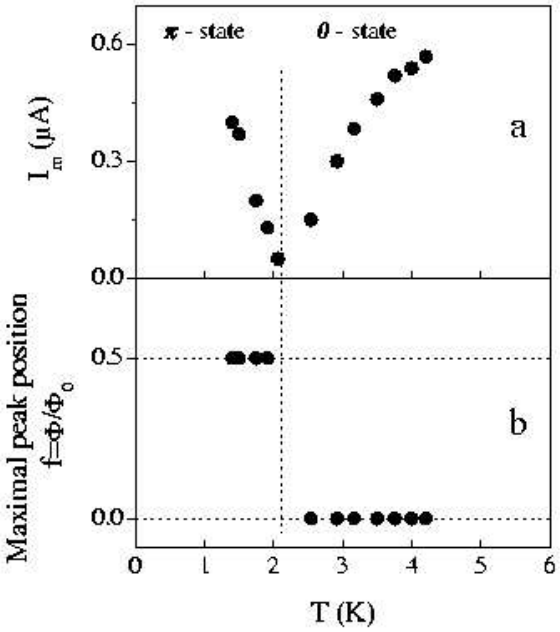

Figure 27: (a) Temperature dependence of the critical transport current for the structure depicted in figure 25 in the absence of magnetic field; (b) temperature dependence (jump) of the position of the maximal peak on the curves $I_m(H)$, corresponding to the two limiting temperatures depicted in figure 26. (From From Ryazanov *et al.* cond-mat/0103240).

parallel one. It happens because the exchange field always suppresses superconductivity. When the fields from different layers are parallel, they enhance this effect and increase the energy, and vice versa. The effect strongly depends on the interfaces transparency. If it is very small, the effect is weak. In the case of almost ideally transparent interfaces the majority electrons with the preferential spin orientation can not penetrate from the F-layer to the S-layer deeper than to the coherence length ξ_s. Therefore, it is reasonable to work with the S-layer whose thickness does not exceed ξ_s. The choice of the material and thickness of F-layers is dictated by the requirement that they could be reoriented by sufficiently weak magnetic field. Thus, the coercive force must be small enough. We refer the reader to the original works for quantitative details.

An alternative approach is to study the thermodynamics of the F/S/F trilayer at a fixed mutual orientation of magnetic moments. Such a study was performed by Baladie and Buzdin [124] for the case of very thin superconducting layer $d_s \ll \xi_s$. They considered F_s almost as a constant, but incorporated small linear and quadratic deviations and solved the linearized Usadel equation as it was shown in subsection 4.2 to find the critical temperature vs. thickness of the ferromagnetic layers. They have found that at large γ_b (low interface transparency) the transition temperature monotonically decreases with d_f increasing from its value in the absence of the F-layers to some saturation value and there is no substantial difference between parallel and antiparallel orientations. At smaller values of γ_b the suppression of T_c increases and at parallel orientation the reentrant transition occurs at $d_f \sim \xi_f$, but still the transition temperature saturates at large d_f. At γ_b smaller than a critical value the transition temperature becomes zero at a finite thickness d_f for both parallel and antiparallel orientation. The authors also have found some evidences that at low γ_b the SC transition becomes discontinuous for the parallel orientation. This conclusion was confirmed by a recent theoretical study by Tollis [126], who has proved that the SC transition for the antiparallel orientation is always of the second order, whereas for the parallel orientation it becomes of the first order for small [126]. Baladie and Buzdin [124] have considered also the energy gap at low temperature. For the case of thick ferromagnetic layers $d_f \gg \xi_f$ they have found that the energy gap is the monotonically decreasing function of the dimensionless collision frequency $(\tau_f \Delta_0)^{-1}$, where Δ_0 is the value of the energy gap in the absence of the ferromagnetic layers. It turns into zero at $(\tau_f \Delta_0)^{-1} = 0.25$ for the parallel and 0.175 for the antiparallel orientation.

4.5 Triplet pairing

If the direction of the magnetization in F-layer is inhomogeneous due to a domain wall or artificially, the singlet Cooper pairs penetrating into the F- from S-layer will be partly transformed into the triplet pairs. This effect was first predicted by Kadigrobov *et al.* [67] and by Bergeret *et al.* [68]. The triplet pairs cannot penetrate to the superconductors over the length larger than magnetic length $l_m = \sqrt{D_f/h}$ (or v_F/h for the clean ferromagnet), but in the ferromagnet they are neither exchange interaction nor the elastic scattering suppresses them. Therefore, they can penetrate over much longer distance $\xi_T = \sqrt{D_f/T}$. Even if the

triplet pairing is weak, it provides the long-range coupling between two superconducting layers in a S/F/S junction. Moreover, if the thickness d_f exceeds l_m significantly, only triplet pairs survive at distances much larger than l_m completely changing the symmetry properties of the superconducting condensate.

The exchange field rotating in the $y-z$-plane is naturally described by the operator in the spin space $\hat{h} = h(\hat{\sigma}_3 \cos\alpha + \hat{\sigma}_2 \sin\alpha)$, where h is a scalar function of coordinates, $\hat{\sigma}_2$ and $\hat{\sigma}_3$ are the Pauli matrices and the angle α is a function of coordinates. It is clear that the non-diagonal part of h flips one of spins of the pair transforming the singlet into the triplet. It does not appear if the magnetization is collinear ($\alpha = 0$). To make things more explicit, let consider the Usadel equation in the F-layer, i.e. equation (38) of the Section (2). First we simplify them by linearization, which is valid if either the transparency of the interface barrier is small [83]. Then the condensate Green tensor $\check{f}$ in F-layer is small. The linearized Usadel equation reads:

$$\frac{D_f}{2}\frac{\partial^2 \check{f}}{\partial z^2} - |\omega|\check{f} + ih\left[\hat{\tau}_0\{\hat{\sigma}_3, \check{f}\cos\alpha + \hat{\tau}_3[\hat{\sigma}_2, \check{f}]\sin\alpha\}\right] = 0, \tag{123}$$

where $\{A, B\}$ means the anticommutator of operators A and B. If $\alpha = const$, equations (123) have an exponential solution $\check{f} = e^{kz}\check{f}_0$. The secular equation for k is:

$$(k^2 - k_\omega^2)^2\left[(k^2 - k_\omega^2)^2 + \frac{2h}{D_f}\right] = 0, \tag{124}$$

where $k_\omega^2 = 2|\omega|/D_f$. Note that the secular equation does not depend on α. It is a consequence of rotational invariance of the exchange interaction. At $\alpha = 0$ the two-fold eigenvalue $k^2 = k_\omega^2$ corresponds to $f_{1,2}$ (triplet pairing with projection ± 1 onto the magnetic field). Since ω_n is proportional to T, these modes are long-range. Two other modes have wave vectors $k = k_h$ and $k = k_h^*$, where $k_h^2 = 2(|\omega| + ih\mathrm{sign}\omega)/D_f$. They penetrate not deeper than on the magnetic length. These short-range modes are linear combinations of the singlet and triplet with spin projection zero, i.e. orthogonal to the magnetic field.

Bergeret *et al.* considered two different geometries. In the first one [68] they considered S/F bilayer. The angle α was a linear function of coordinate starting from 0 at the S/F interface, reaching a value α_w at the distance w from the interface and remaining constant at larger distances. They have solved the linearized Usadel equation (123) with the boundary condition $\xi_f \frac{dF_f}{dz} = \gamma_b F_s$ proper at small transparency of the interface by a clever unitary transformation $\check{f} \to \hat{U}(z)\check{f}[\hat{U}(z)]^{-1}$ with $\hat{U}(z) = \exp(iQ\hat{\sigma}_1 z/2)$ and $Q = \frac{d\alpha}{dz} = \frac{\alpha_w}{w}$. This transformation turns the rotating magnetic field into the constant one, directed along z-axis, but differential term generates perturbations proportional to Q and Q^2. By this trick the initial equations with the coordinate dependent $\check{h}(z)$ is transformed into an ordinary differential equation with constant (operator) coefficients. The generation of the triplet component is weak if γ_b is large and it acquires an additional small factor if the ratio ξ_f/w is small (w mimics the domain wall width), but, as we have demonstrated, this component has a large penetration depth. Experimentally it could produce a strong enhancement of the F-layer conductivity. Such an enhancement was observed in the experiment by Petrashov *et al.*[127] in 1999, two

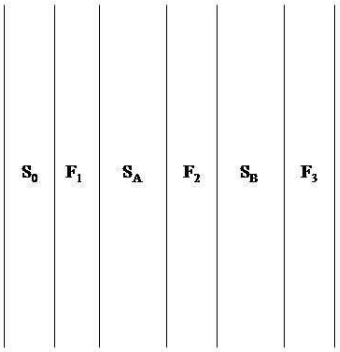

Figure 28: 6-layer structure.

years afore the theoretical works. They studied an F/S bilayer made from 40nm thick Ni and 55nm thick Al films. The interface was about 100x100nm^2. The samples were prepared by e-beam lithography. They measured the resistivity and the barrier resistance directly. They have found also the diffusion coefficients $D_s = 100cm^2/s$ and $D_f = 10cm^2/s$, which we cite here to give an idea about the order of magnitudes. They have found a large drop of the resistance of the sample, which could not be explained by the existing singlet pairing mechanism. We are not aware about the detailed comparison of the theory [68] and the experiment [127]. One more evidence of long range penetration of the superconducting order parameter through the ferromagnet was reported in [128]. The authors measured the resistance of $0.5\mu m$ Ni loop connected with superconducting Al wire. They extracted the decay length for proximity effect in ferromagnet from differential resistance and concluded that it is much larger than it could be expected for singlet pairing.

In their second work on the triplet pairing [83] the authors have proposed an interesting 6-layer structure presented in figure 28. The assume that the magnetization in each layer is constant, but its direction is different in different layers. It is supposed to lay in the $y-z$-plane and thus it can characterized by one angle. Let this angle is $-\alpha$ in the layer F_1, 0 in the layer F_2 and $\pm\alpha$ in the layer F_3. They speak about the positive chirality if the sign is $+$ and negative chirality if the sign is $-$. They prove that, if the thickness of F-layers is larger than l_m, the superconducting layers S_A and S_B are connected by 0-junction if the chirality is positive and by π-junction if the chirality is negative. This phenomenon is completely due to the triplet pairing since it dominates on this distance. Kulic and Kulic [129] considered two bulk magnetic superconductors with rotating magnetization separated by an insulating layer. They also have found that the sign of the Josephson current can be negative depending on the relative chirality. In this system singlet and triplet pairs coexist in the bulk, whereas in

the system proposed by Bergeret *et al.* the triplet dominates. We will give a brief description how did they derive their results. They solved the Usadel equation in each layer separately (it can be done without linearization, since the coefficients of the differential equations are constant) and match these solutions using the Kupriyanov-Lukichev boundary conditions. The current density in the F_2 layer can be calculated using the modified Eilenberger-Usadel expression:

$$j = \sigma_f \mathrm{Tr}\left(\hat{\tau}_3\hat{\sigma}_0\pi T\sum_{\omega_n}\check{f}\frac{d\check{f}}{dz}\right) \tag{125}$$

The maximal effect is reached when magnetic moment of the central layer is perpendicular to two others.

5 Conclusions

This short review shows that though the studies of Ferromagnet-Superconductor Hybrids are coming of age, we are at the beginning of interesting voyage into this emerging field. The most active development undoubtedly take place in the field of proximity based phenomena in layered ferromagnet-superconductor systems. The strong point of this thrust is fruitful collaboration between experiment and theory. This progress was achieved due to a new idea due to Ryazanov and coworkers to use the weak ferromagnets in th experiment. This idea allowed to increase the thickness of ferromagnetic layers to a macrosopic scale and simultaneously allowing to drive the non-monotonous behavior of the Josephson current by temperature. On this way experimenters have reliably found several interesting phenomena predicted many years ago, as $0-\pi$-transition and oscillations of critical temperature vs. the thickness of the F-layer and also some new phenomena as the valve effect in F/S/F junction and the Shapiro steps at half- integer frequencies.

The experimental studies of ordering/transport in FSH have greatly benefited with introduction of imaging technique (SHPM,MFM) in the field. We expect that several experimental groups will get access to this technique in the near future which will result in more exciting experiments. The theoretical and experimental studies of ordering/transport in FSH have surprisingly little overlap, especially in comparison with studies of proximity based phenomena. The materials used in the experiment are far from being regular, whereas the theorist so far preferred simple problems with regular, homogeneous or periodical systems. Even the simplest idea about topological instability in the S/F-bilayer was not checked experimentally. It would be very instructive to find experimentally the phase diagram of a single magnetic dot using the SQUID magnetometer or the MFM. Finally the transport properties of the S/F- bilayer and the S-films supplied with regular or randomly magnetized arrays of F-dots should be measured. On the other hand the experiment dictates new problems for theory: a description of random set of strongly pinned domain walls, their magnetic field and its effect on the S-films. We think that both experimental and theoretical communities can find systems of common interests. Another possibility for interesting development in the FSH field we expect with introduction of new types of FSH, e.g. arrays of magnetic nanowires in

alumina templates, covered with superconducting film. Such arrays provides alternative to magnetic dots source of alternating magnetic field of high strength and short scale variation.

6 Acknowledgements

The authors acknowledge the support by NSF under the grants DMR-0103455 and DMR-0321572, by DOE under the grant DE-FG03-96ER45598, by Telecommunications and Informatics Task Force at Texas A&M University and by Deutsche Forschungsgemeinschaft. V.P. acknowledges the support from the Humboldt Foundation, Germany. He is indebted to the University of Cologne and to Prof. T. Nattermann for the hospitality during his stay in Cologne, where a part of this work was performed. I.L. is grateful to Prof. H. Pfnür, for kind hospitality during stay at Hannover University, where part of the work has been done.

References

[1] Fischer, O. , *Magnetic Superconductors* in Ferromagnetic Materials V. 5, K.H.J. Buschow and E.P. Wohlfarth, eds. (North-Holland, Amsterdam, 1990) pp. 465-549.

[2] Bulaevskii, L. N., Buzdin, A. I., Kulic, M. L., and Panyukov, S. V., 1985, *Adv. Phys.*, **34**, 175.

[3] Otani, Y., Pannetier, B., Nozieres, J. P., and Givord, D., 1993, *J. Magn. Mag. Mat.*, **126**, 622.

[4] Geoffroy, O., Givord, D., Otani, Y., Pannetier, B., and Ossart, F., 1993, *J. Magn. Magn. Mater.*, **121**, 223.

[5] Nozaki, Y., Otani, Y., Runge, K., Miyajima, H., Pannetier, B., Nozieres, J. P., and Fillon, G., 1996, *J. Appl. Phys.*, **79**, 8571.

[6] Martin, J. I. , Velez, M. , Nogues, J., and Schuller, I. K. , 1997, *Phys. Rev. Lett.*, **79**, 1929.

[7] Morgan, D. J., and Ketterson, J. B., 1998, *Phys. Rev. Lett.*, **80**, 3614.

[8] Daldini, O., Martinoli, P., Olsen, J. L., and Berner, G., 1974, *Phys. Rev. Lett.*, **32**, 218.

[9] Daldini, O., Leemann, C., and Martinoli, P., 1975, *Helv.Phys.Acta*, **48**, 2.

[10] Martinoli, P., Nsabimana, M., Racine, G. A., Beck, H., and Clem, R., 1983, *Helv.Phys.Acta*, **56**, 765.

[11] Hebard, A. F., Fiory, A. T., and Somekh, S., 1977, *IEEE T. Magn.*, **13**, 589.

[12] Fiory, A. T., Hebard, A. F., and Somekh, S., 1978, *App. Phys. Lett.*, **32**, 73.

[13] Metlushko, V. V., Baert, M., Janckheere, R., Moshchalkov, V. V., and Bruynserade, Y., 1994, *Solid State Comm.*, **91**, 331.

[14] Baert, M., Metlushko, V. V., Janckheere, R., Moshchalkov, V. V., and Bruynserade, Y., 1995, *Phys. Rev. Lett.*, **74**, 3269.

[15] Moschalkov, V. V., Baert, M., Metlushko, V. V., Rosseel, E., Van Bael, M. J., Temst, K., Janckheere, R., and Bruynserade, Y., 1996, *Phys. Rev.* B, **54**, 7385.

[16] Harada, K., Kamimura, O., Kasai, H., Matsuda, T., Tonomura, A., and Moshchalkov, V. V., 1996, *Science*, **274**, 1167.

[17] Metlushko, V. V., DeLong, L. E., Baert, M., Rosseel, E., Van Bael, M. J., Temst, K., Moshchalkov, V. V., and Bruynseraede, Y., 1998, *Europhys. Lett.*, **41**, 333.

[18] Moshchalkov, V. V., Baert, M., Metlushko, V. V., Rosseel, E., Van Bael, M. J., Temst, K., Bruynseraede, Y., and Jonckheere, R., 1998, *Phys. Rev.* B, **57**, 3615.

[19] Van Bael, M. J., Temst, K., Moshchalkov, V. V., and Bruynseraede, Y., 1999, *Phys. Rev.* B, **59**, 14 674.

[20] Pokrovsky, V. L., and Talapov, A. L., 1984, *Theory of Incommensurate Crystals* (Harwood Academic Publishers, NY).

[21] Pokrovsky, V. L., Talapov, A. L., and Bak, P., 1996, *Thermodynamics of Two-dimensional Soliton Systems*, in Solitons S. E. Trullinger, V. E. Zakharov, and V. L. Pokrovsky editors,(North-Holland, NY)

[22] Beck, H., Simanek, F., Puga, M., Martinoli, P., Nsabimana, M., and Racine, G. A., 1981, *Helv. Phys. Acta*, **54**, 651.

[23] Van Bael, M. J., Bekaert, J., Temst, K., Van Look, L., Moshchalkov, V. V., Bruynseraede, Y., Howells, G. D., Grigorenko, A. N., Bending, S. J., and Borghs, G., 2001, *Phys. Rev. Lett.*, **86**, 155.

[24] Lange, M., Van Bael, M. J., Van Look, L., Temst, K., Swerts, J., Guntherodt, G., Moshchalkov, V. V., and Bruynseraede, Y., 2001, *Europhys. Lett.*, **51**, 110.

[25] Bending, S. J., Howells, G. D., Grigorenko, A. N., Van Bael, M. J., Bekaert, J., Temst, K., Van Look, L., Moshchalkov, V. V., Bruynseraede, Y., Borghs, G., and Humphreys, R. G., 2000, *Physica* C, **332**, 20.

[26] Lyuksyutov, I. F., and Pokrovsky, V. L., 1998, *Phys. Rev. Lett.*, **81**, 2344.

[27] Lyuksyutov, I. F., and Pokrovsky, V. L., 1998, *Magnetism Coupled Vortex Matter* in Proc. SPIE Vol.3480, p. 230-235, *Superconducting Superlattices II: Native and Artificial.* Ivan Bozovic and Davor Pavuna Eds.

[28] Lyuksyutov, I. F., Naugle, D. G., and Pokrovsky, V. L., 2000, *Frozen Flux Superconductors*, Proc. SPIE Vol. 4058, p. 376-387, *Superconducting and Related Oxides: Physics and Nanoengineering IV*, D. Pavuna and I. Bozovic, Eds.

[29] Feldman, D. E., Lyuksyutov, I. F., Pokrovsky, V. L., and Vinokur, V. M., 2000, *Europhys. Lett.*, **51**, 110.

[30] Lyuksyutov, I. F., and Pokrovsky, V. L., 1999, cond-mat/9903312, 2000, *Mod. Phys. Lett.* B, **14**, 409.

[31] Erdin, S., Lyuksyutov, I. F., Pokrovsky, V. L., and Vinokur, V. M., 2002, *Phys. Rev. Lett.*, **88**, 017001.

[32] Erdin, S., Kayali, M. A., Lyuksyutov, I. F., and Pokrovsky, V. L., 2001, *Phys. Rev.* B, **66**, 014414.

[33] Pokrovsky, V. L., and Wei, H., 2004, *Phys. Rev.* B, **69**, 104530.

[34] Kayali, M. A., and Pokrovsky, V. L., 2004, *Phys. Rev.* B, **69**, 132501.

[35] Lyuksyutov, I. F., and Naugle, D. G., 1999, *Modern Phys. Lett.* B, **13**, 491.

[36] Lyuksyutov, I. F., and Naugle, D. G., 2000, *Physica* C, **341-348**, 1267.

[37] Lyuksyutov, I. F., and Naugle, D. G., 2003, *J. Mod. Phys.* B, **17**, 3441.

[38] Lyuksyutov, I. F., and Naugle, D. G., 2003, *J. Mod. Phys.* B, **17**, 3713.

[39] Santos, J. E., Frey, E., and Schwabl, F., 2001, *Phys. Rev.* B, **63**, 4439.

[40] Sasik, R., and Hwa, T., 2000, Preprint cond-mat/0003462.

[41] Marmorkos, I. K., Matulis, A., and Peeters, F. M., 1996, *Phys. Rev.* B, **53**, 2677.

[42] Milosevic, M. V., Yampolskii, S. V., and Peeters, F. M., 2002, *Phys. Rev.* B, **66**, 174519.

[43] Milosevic, M. V., and Peeters, F. M., 2003, *Phys. Rev.* B, **68**, 094510.

[44] Milosevic, M. V., and Peeters, F. M., 2004, *Phys. Rev.* B, **69**, 104522.

[45] Kayali, M. A., 2004, *Phys. Rev.* B, **69**, 012505.

[46] Erdin, S., 2003, *Physica* C, **391**, 140.

[47] Bulaevskii, L. N., and Chudnovsky, E. M., 2000, *Phys. Rev.* B, **63**, 012502.

[48] Sonin, E. B., 2002, *Phys. Rev.* B, **66**, 136501.

[49] Laiho, R., Lähderanta, E., Sonin, E. B., and Traito, K. B., 2003, *Phys. Rev.* B, **67**, 144522.

[50] Traito, K. B., Laiho, R., Lähderanta, E., and Sonin, E. B., 2003, *Physica* C, **388**, 641.

[51] Helseth, L. E., Goa, P. E., Hauglin, H., Baziljevich, M., and Johansen, T. H., 2002, *Phys. Rev.* B, **65**, 132514.

[52] Aladyshkin, A. Yu., Buzdin, A. I., Fraerman, A. A., Melnikov, A. S., Ryzhov, D. A., and Sokolov, A. V., 2003, *Phys. Rev.* B, **68**, 184508.

[53] Larkin, A. I., and Ovchinnikov, Yu. N., 1965, *Zh. Exp. Teor. Fiz.*, **47**, 1136, [1965, *Sov. Phys. JETP*, **20**, 745].

[54] Fulde, P., and Ferrel, R. A., 1965, *Phys. Rev.*, **135**, 550.

[55] Bulaevskii, L. N., Kuzii, V. V., and Sobyanin, A. A., 1977, *Pis'ma ZhETF*, **25**, 314, [1977, *Sov. Phys. JETP Lett.*, **7**, 290].

[56] Buzdin, A. I., Bulaevskii, L. N., and Panyukov, S. V., 1982, *Pis'ma ZhETF*, **35**, 147, [1982, *JETP Lett.*, **35**, 178.]

[57] Ryazanov, V. V., Oboznov, V. A., Rusanov, A. Yu., Veretennikov, A. V., Golubov, A. A., and Aarts, J., 2001, *Phys. Rev. Lett.*, **86**, 2427.

[58] Ryazanov, V. V., Oboznov, V. A., Veretennikov, A. V., and Rusanov, A. Yu., 2001, *Phys. Rev.* B, **65**, 020501.

[59] Kontos, T., Aprili, M., Lesueur, J., Genet, F., Stephanides, B., and Boursier, R., 2002, *Phys. Rev. Lett.*, **89**, 137007.

[60] Izyumov, Yu. A., Proshin, Yu. N., and Khusainov, M. G., 2002, *Sov. Phys. Uspekhi*, **45**, 109.

[61] Garifullin, I. A., 2002, *J. Magn. Magn. Mat.*, **240**, 571.

[62] Buzdin, A. I., and Kupiyanov, M. V., 1990, *Pis'ma Zh. Exp. Teor. Fiz.,* **52**, 1089, [1990, *Sov. Phys. JETP Lett.*, **52**, 487.]

[63] Radovic, Z., Ledwij, M., Dobroslawljewich-Grujich, Lj., Buzdin, A. I., and Clem, J. R., 1991, *Phys. Rev.* B, **44**, 759.

[64] Sa de Melo, C. A. R., 1997, *Phys. Rev. Lett.*, **79**, 1933.

[65] Buzdin, A. I., Vedyaev, A. V., and Ryzhanova, N. V., 1999, *Europhys. Lett.,* **48**, 686.

[66] Tagirov, L. R., 1999, *Phys. Rev. Lett.,* **83**, 2058.

[67] Kadigrobov, A., Shekhter, R. I., and Johnson, M., 2001, *Europhys. Lett.,* **54**, 394.

[68] Bergeret, F. S., Volkov, A. F., and Efetov, K. B., 2001, *Phys. Rev. Lett.,* **86**, 4096.

[69] Ioffe, L. B., Geshkenbein, V. B., Feigelman, M. V., Fauchere, A. L., and Blatter, G., 1999, *Nature,* **398**, 679.

[70] Eom, J., and Johnson, M., 2001, *Appl. Phys. Lett.,* **79**, 2486.

[71] Abrikosov, A. A. 1986, *Introduction to the Theory of Metals*, (North Holland, Amsterdam).

[72] Pearl, J., 1964, *J. Appl. Phys. Lett.,* **5**, 65.

[73] Bogolyubov, N. N., 1958, *Zh. Eksp. Teor. Fiz.*, **34**, 58; **34**, 73; [1958, *Sov. Phys. JETP*, **7**, 41; 1958, **7**, 51].

[74] de Gennes, P. G., 1964, *Rev. Mod. Phys.*, **36**, 225.

[75] Gor'kov, L.P., 1958, *Zh. Exp. Teor. Fiz.,* **34**, 735, [1958, *Sov. Phys. JETP*, **7**, 505].

[76] Ryazanov, V. V., Oboznov, V. A., Veretennikov, A. V., Rusanov, A. Yu., Golubov, A. A., and Aarts, J., 2001, *Usp. Fiz. Nauk.*, **171**, 81.

[77] Eilenberger, G., 1968, *Z. f. Physik*, **214**, 195.

[78] Larkin, A. I., and Ovchinnikov, Yu. N., 1965, *Sov. Phys. JETP,* **20**, 762.

[79] Usadel, K., 1970, *Phys. Rev. Lett.,* **25**, 507.

[80] Tinkham, M., 1996, *Introduction to Superconductivity*, (Mc-Graw-Hill, New York).

[81] Kopnin, N. B., 2001, *Theory of Nonequilibrium Superconductivity*, (Oxford University Press).

[82] Abrikosov, A. A., Gor'kov, L. P., and Dzyaloshinskii, I. E., *Methods of Quantum Field Theory in Statistical Physics*, (Dover, New York, 1977).

[83] Bergeret, F.S., Efetov, K. B., and Volkov, A. F., 2003, *Phys. Rev.* B, **68**, 064513.

[84] Zaitsev, A. V., 1984, *Zh. Exp. Teor. Fiz.,* **86**, 1742, [1985, *Sov. Phys. JETP,* **59**, 1015].

[85] Kupriyanov, M. Yu., and Lukichev, V. F., 1988, *Zh. Exp. Teor. Fiz.,* **94**, 139. [1988, *Sov. Phys. JETP,* **67**, 1163].

[86] Baladie, I., Buzdin, A. I., Ryzhanova, N. V., and Vedyaev, A. V., 2001, *Phys. Rev.* B, **63**, 054518.

[87] Van Bael, M. J., Bekaert, J., Temst, K., Van Look, L., Moshchalkov, V. V., Bruynseraede, Y., Howells, G. D., Grigorenko, A. N., Bending, S. J., and Borghs, G., 2001, *Phys. Rev. Lett.*, **86**, 155.

[88] Van Bael, M. J., Lange, M., Raedts, S., Moshchalkov, V. V., Grigorenko, A. N., and Bending, S. J., 2003, *Phys. Rev.* B, **68**, 014509.

[89] Moshchalkov, V. V., Baert, M., Metlushko, V. V., Rosseel, E., Van Bael, M. J., Temst, K., and Bruynseraede, Y., 1998, *Phys. Rev.* B, **57**, 3615.

[90] Lange, M., Van Bael, M. J., Bruynserade, Y., and Moshchalkov, V. M., 2003, *Phys. Rev. Lett.*, **90**, 197006.

[91] Lyuksyutov, I. F., 2002, *Mod. Phys. Lett.*, B **16**, 569.

[92] Bardeen, J., and Stephen, M. J., 1969, *Phys. Rev.*, **140**, 1197A.

[93] de Gennes, P. G., 1989, *Superconductivity of Metals and Alloys* (Addison-Wesley, New York).

[94] Yafet, Y., and Gyorgy, E. M., 1988, *Phys. Rev.* B, **38**, 9145.

[95] Kaplan, B., and Gehring, G. A., 1993, *J. Magn. Magn. Mater.,* **128**, 111.

[96] Allenspach, R., 1995, *J. Magn. Magn. Mater.,* **129**, 160.

[97] Portmann, O., Vaterlaus, A., and Pescia, D., 2003, *Nature,* **422**, 701.

[98] Lange, M., Van Bael, M. J., Moshchalkov, V. V., and Bruynseraede, Y., 2002, *Appl. Phys. Lett.,* **81**, 322.

[99] Lange, M., Van Bael, M. J., and Moshchalkov, V. V., 2003, *Phys. Rev.,* B, **68**, 174522.

[100] Lange, M., Moshchalkov, V. V., and Van Bael, M. J., 2003, *Mod. Phys. Lett.*, B **17**, 519.

[101] Sonin, E. B., 1988, *Pis'ma Zh. Tekh. Fiz.,* **14** 1640, [1988, *Sov. Tech. Phys. Lett.,* **14**, 714.].

[102] Demler, E. A., Arnold, G. B., and Beasley, M. R., 1999, *Phys. Rev.* B, **55**, 15174.

[103] Andreev, A. F., 1964, *Pis'ma ZhETF,* **46**, 1823, [1964, *Sov. Phys. JETP Lett.,* **19**, 1228.]

[104] Blonder, G. E., Tinkham, M., and Klapwijk, T. M., 1982, *Phys. Rev.* B, **25**, 4515.

[105] Fominov, Ya. V., Chtchelkachev, N. M., and Golubov, A. A., 2002, *Phys. Rev.* B, **66**, 014507.

[106] Proshin, Yu. N., and Khusainov, M. G., 1998, *Zh. Exp. Teor. Fiz.,* **113**, 1708, [1998, *Sov. Phys. JETP,* **86**, 930].

[107] Jiang, J. S., Davidovic, D., Reich, D. H., and Chien, C. L., 1995, *Phys. Rev. Lett.,* **74**, 314; 1996, *Phys. Rev.* B, **54**, 6119.

[108] Mühge, Th., Garifyanov, N. N., Goryunov, Yu. V., Khaliullin, G. G., Tagirov, L. R., Westerholt, K., Garifullin, I. A., and Zabel, H., 1996, *Phys. Rev. Lett.,* **77**, 857.

[109] Aarts, J., Geers, J. M. E., Brück, E., Golubov, A. A., and Goehorn, R., 1997, *Phys. Rev.* B, **56**, 2279.

[110] Lazar, L., Westerholt, K., Zabel, H., Tagirov, L. R., Goryunov, Yu. V., Garifyanov, N. N., and Galifullin, I. A., 2000, *Phys. Rev.* B, **61**, 3711.

[111] Rusanov, A., Boogaard, R., Hesselberth, M., Seiler, H., and Aarts, J., 2002, *Physica* C, **369**, 300.

[112] Ryazanov, V. V., Oboznov, V. A., Prokofiev, A. S., and Dubonos, S. V., 2003, *Pis'ma Zh. Exp. Teor. Fiz.,* **77**, 43; [2003, *JETP Letters,* **77**, 39].

[113] Tagirov, L. R., 1998, *Physica* C, **307**, 145.

[114] Buzdin, A. I., Vujicic, B., and Kupriyanov, M. Yu., 1992, *Zh. Exp. Teor. Fiz.,* **101**, 231; [1992, *Sov. Phys. JETP,* **74**, 124].

[115] Heikkilä, T. T., Wilhelm, F. K., and Schön, G., 2000, *Europhys. Lett.,* **51**, 434.

[116] Buzdin, A., and Baladie, I., 2003, *Phys. Rev.* B, **67**, 184519.

[117] Zyuzin, A. Yu., Spivak, B, and Hruska, M. 2003, *Europhys. Lett.,* **62**, 97.

[118] Radovic, Z., Lazarides, N., and Flytzanis, N., 2003, *Phys. Rev.* B, **68**, 014501.

[119] Halterman, K., and Valls, O. T., 2002, *Phys. Rev.* B, **66**, 224516; 2004, *Phys. Rev.* B, **69**, 014517.

[120] Bergeret, F. S., Volkov, A. F., and Efetov, K. B., 2001, *Phys. Rev.* B, **64**, 134506.

[121] Sellier, H., Baraduc, C., Lefloch, F., and Galemczuk, R., 2004, cond-mat/0406236.

[122] Grünberg, P., Schreiber, R., Pang, Y., Brodsky, M. B., and Sowers, H., 1986, *Phys. Rev. Lett.,* **57**, 2442.

[123] Parkin, S. S. P., More, N., and Roche, K. P., 1990, *Phys. Rev. Lett.,* **64**, 2304.

[124] Baladie, I., and Buzdin, A. I., 2003, *Phys. Rev.* B, **67**, 014523.

[125] Tagirov, L. R., Garifullin, L. A., Garifyanov, N. N., Khlebnikov, S. Ya., Tikhonov, D. A., Westerholt, K., and Zabel, H., 2002, *J. Magn. Magn. Mater.,* **240**, 577.

[126] Tollis, S., 2004, *Phys. Rev.* B, **69**, 105432.

[127] Petrashov, V. T., Sosnin, I. A., Cox, I., Parsons, A., and Troadec, C., 1999, *Phys. Rev. Lett.,* **83**, 3281.

[128] Giroud, M., Cortois, H., Hasselbach, K., Mailly, D., and Pannetier, B., 1998, *Phys. Rev.* B, **58**, R11872.

[129] Kulic, M. L., and Kulic, I. M., 2001, *Phys. Rev.* B, **63**, 104503.